DLR-IB-FA-BS-2018-118

Analyse und Auswahl von Strukturkonzepten für den strukturellen Tragflügelentwurf

Diplomarbeit

Niklas Ulff, Sascha Dähne

Deutsches Zentrum für Luft- und Raumfahrt

MH-FA-56-FB03_v1.3

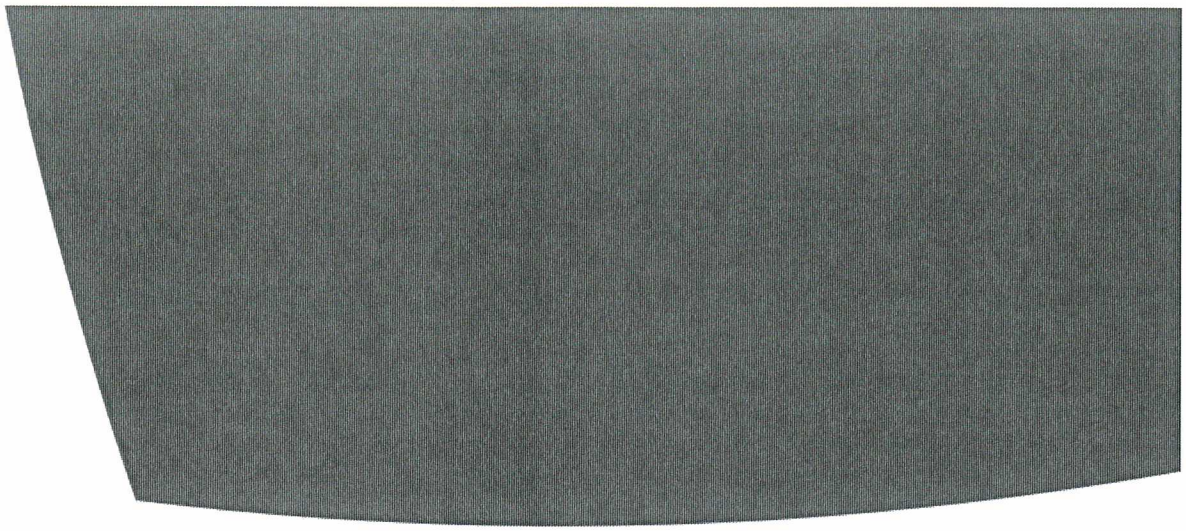

Institut für Faserverbundleichtbau und Adaptronik

DLR-IB-FA-BS-2018-118

Analyse und Auswahl von Strukturkonzepten für den strukturellen Tragflügelentwurf

Zugänglichkeit:

Stufe 2 DLR intern zugänglich

Braunschweig, *August, 2018*

Der Bericht umfasst: 94 Seiten

Abteilungsleiter:

Prof. Dr.-Ing. Christian Hühne

Autoren: *Niklas Ulff*

Autor 2 / Betreuer: Sascha Dähne

Deutsches Zentrum für Luft- und Raumfahrt

Abstract

The Institute of Composite Structures and Adaptive Systems at the German Aerospace Center (DLR) developed a process to evaluate the structural wing design, by "smearing" the stringer into a shell model with equivalent-plate stiffness. To extend the present method, this thesis seeks to implement further stiffening concepts. To achieve this objective, the aircraft wing is first analyzed and required load-paths, as well as components for the structural design are determined. The outlined components of interest, are then described by an equivalent-plate stiffness and implemented into the method. Subsequently, stiffening concepts are evaluated to pre-defined criteria and an eligible selection is then validated with respect to discrete FE-models. Finally, conducted optimization runs show, that the derived equivalent stiffness formulation is an appropriate way to analyze the stiffened skin panels and minimize the weight, while sustaining defined constraint functions in terms of critical failure modes.

Kurzfassung

Das Institut für Faserverbundleichtbau und Adaptronik hat für die Auslegung versteifter Hautstrukturen einen semi-analytischen Prozess aufgebaut und eine Parametrisierung versteifter Paneele auf Basis von verschmierten Platten-Steifigkeiten entwickelt. Das Ziel der vorliegenden Arbeit ist, den vorhandenen Prozess zu erweitern und weitere Versteifunselemente zu ergänzen. Dazu wird zunächst die Auslegung von Flügelstrukturen analysiert, um resultierende Kraftpfade zu bestimmmen und Strukturkonzepte werden herausgearbeitet. Die definierten Strukturen sollen dann, in Anlehnung an den bereits vorhandenen Prozess, in ein Schalenmodell mit equivalenter Steifigkeit verschmiert werden. Bestimmte Konzepte, die anhand von definierten Kriterien ausgewählt wurden, werden dann in den Basisprozess implementiert und anschließen mit diskreeten FE-Modellen validiert. Im Anschluss zeigen Optimierungsdurchläufe, dass equivalente Schalenmodelle sehr gut geeignet sind, um Flügelkonzepte hinsichtlich Gewichtsminimierung zu analysieren, während Fehlerkriterien eingehalten werden.

Contents

List of Abbreviations

AC Aerodynamic Center

CP Center of Pressure

CFRP Carbon Fibre Reinforced Plastics

CLT Classical Lamination Theory

DLR German Aerospace Center (DLR)

FE Finite Elements

PREPREG Pre-Impregnated Material

ATL Automated Tape Laying

PRTM Pultrusion Resin Transfer Molding

ASF Automated Stiffener Forming

MHI Mitsubishi Heavy Industries

MPC Multiple Point Constraint

NEF No-Edge-Free

OEF One-Edge-Free

List of Symbols

Latin Symbol	**Property**	**Unit**
$\boldsymbol{ABD}$	ABD matrix	-
A	Cross-section area	mm
E	Young's modulus of elasticity	$\mathrm{N\,mm^{-2}}$
E_S	Effective axial modulus	$\mathrm{N\,mm^{-2}}$
G	Shear modulus	$\mathrm{N\,mm^{-2}}$
I	Second moment of inertia	$\mathrm{mm^4}$
I_t	Torsional rigidity	$\mathrm{mm^4}$
J_S	Effective torsional constant	$\mathrm{mm^4}$
$\boldsymbol{T}$	Transformation matrix	-
a, b	Dimensions for plate	mm
d_s	Stiffener spacing	mm
t	Thickness	mm
$k_\mathrm{y}, k_\mathrm{z}$	In-plane and transverse shear correction factor	-
h	Height of stiffener	mm
n_s	Number of stiffener on panel	-
w	Width	mm

Greek Symbol	**Property**	**Unit**
φ	Slope of web for closed cross-sections	$^\circ$
ν	Poisson's ratio	-
ε	Laminate's strains	-
γ	Laminate's strains	-

Subscripts	**Property**
cs	Closed span - Span between webs of closed stiffening profiles
ss	Spacing span - Span between webs including the foot
os	Open span - Span between webs or if present between feet of stiffening structures
crown	Flange of closed section profiles
skin	Flat plate which is stiffened by stringer
stiffener	Cross-section to stiffen the plate, respectively skin
flange	Flange of open section profiles
(left, right) web	Web of open and closed section profiles
(left, right) foot	Foot of open and closed section profiles
panel	Combination of stiffener and skin

1. Introduction

The commercial aircraft industry and market is constantly growing and according to Airbus' [43] and Boeing's [7] global market forecast, it will continue to do so. To meet the higher demand for aircraft and especially for their increased efficiency, manufactures work intensively on improving established aircraft types and adjusting them to create new generations, specifically by reducing weight through new materials. To achieve this goal, the use of composite materials for high-tech structures became an inevitable choice for designers, to develop more efficient and environmentally friendly airplanes. By replacing secondary structural elements step-wise, they gathered information about the new materials and studied their behavior under operational conditions. Subsequently, greater amount of components could be replaced, as a result of new developments and the ability to produce larger and more complex structures. Referring to Breuer [8], the orthotropic behavior of such materials, meaning directional depended stiffness properties, allows tailored solutions for particular load paths. Consequently, designs can be achieved with a high stiffness-to-weight ratio which leads to efficient and lightweight design, in comparison to conventional metal structures.

To utilize the advantages of composite materials, specifically for aerospace applications, the Institute of Composite Structures and Adaptive Systems at the German Aerospace Center (DLR) in Brunswick researches this topic with high interest. Several on-going projects explore the feasibility, especially of carbon fibre reinforced plastics (CFRP), for primary structures, such as fuselage and wings. One internal project focuses on conducting optimization studies for long-range commercial aircraft in particular and its goal is to optimize the structure to achieve a lightweight design. Thus, to gain a detailed perspective, this work analyzes structural wing concepts as part of the mentioned ongoing research.

1.1. Motivation

To conduct preliminary studies of structural wing design, large amount of data has to be processed, since the design depends on various variables. Structural analyses are usually conducted with numerical solutions, i.e., finite element (FE) analyses, to determine deformation and occurring stresses. However, aircraft structures and in particular wing panels, have multiple curved surfaces and changing the stiffeners geometry results in complex modeling. Furthermore, altering the geometry requires re-meshing the model, which is not just inefficient, it also influences the outcome. Hence, every new mesh can slightly change the computed solution, thus, it is not accurately predictable whether the new geometry or new mesh alters the result, especially when it comes to small changes. To improve performance of preliminary studies of structural wing design, discrete components, such as wing panel stringers, are sought to be simplified by "smearing" the stringer into an equivalent-layer. The equivalent-layer is then superimposed with the skin and represented by so-called shell models. This leads to two remarkable advantages. Firstly, the equivalent-layer as well es the skin's stiffness can be described by an analytical formulation which is assigned to the shell model. The shell model's mesh does not have to be redefined. Secondly, the obtained analytical stiffness matrix, which considers dimensions and material properties of the skin and stringer, can be optimized in terms of minimizing an objective function with mathematical operations.

However, the current in-house optimization environment was initially developed for aircraft designs made of conventional isotropic materials. Although it was extended with the ability to handle orthotropic materials, thus, composite materials, it is based on outdated methods and needs to be replaced, therefore, a new optimization environment is under development, which specifically takes into consideration both isotropic as well as orthotropic materials to minimize the stiffness formulation for the shell element in terms of lightweight designs.

Recent researches have shown, that various approaches exist to accomplish the objective. Bisagni and Vesconi [6] presented a method based on a genetic algorithm which optimizes the function to local and global buckling constraints. However, genetic algorithms have certain limitations when it comes to handling a high number of variables. When the objective function includes a great set of variables, a gradient based approach is generally a better solution. Khani et al. [27] and IJsselmuiden et al. [24] for example, used this method to conducted failure strength analyses. Barkanov et al. [4, 5] and Herencia et al. [23] published a gradient based approach to optimize stiffened panels with respect to buckling criteria.

Dähne and Hühne [13, 14] from the Institute of Composite Structures and Adaptive System at DLR in Brunswick have successfully shown the proof of concept for a gradient base optimization method. They conducted studies for determining the deflection of a rectangular wing box stiffened with blade stringers and subjected to external loads inside a newly developed optimization environment. In this work, the initial approach is enhanced to implement further stiffening concepts and more importantly, to improve the present method by combining various theories.

1.2. Problem Statement

The problem statement of this thesis is, to define an analytical equivalent stiffness formulation, which describes the structural wing design with so-called shell elements. The currently developed method at DLR is however, limited to determine the equivalent formulation for skins, braced by simple blade-stringers. To extend the feasibility of the currently developed design method for the structural wing design, this work seeks to implement further stiffening concepts.

Therefore, an analytical formulation must be derived to describe the stiffened skin panel with an equivalent-plate stiffness formulation. Furthermore, the formulation must be eligible to work inside an optimization environment, since the base idea of modeling the wing with shell elements is supposed to allow parameter and feasibility studies. Analytical formulations, however, are always based on assumptions and simplifications, which not necessarily comply with numerical solutions, for example the numerical discrete wing model. Thus, to verify the derived analytical solution and show its validity, sources of errors and inaccuracies must be determined.

The followed approach in this thesis is on the one hand to smear the stringer into and equivalent-plate layer and superimpose its properties with the skin and on the other, to show its validity to work inside the optimization method. Therefore, the thesis is structured as follows.

Chapter 2 introduces the necessary background information of structural aircraft wing design. Chapter 3 deals with the analytical formulation to describe the shell's equivalent properties. In Chapter 4, a selection of eligible stiffening concepts is made and in Chapter 5 validated with respect to discrete FE models. Chapter 6 finally utilizes the derived formulation and a stiffened panel is optimized in terms of minimizing the weight.

2. Background

This chapter gives a broad overview of the structural design of aircraft, more specifically, the primary components of the wing. Therefore, Section 2.1 discusses the fundamentals of wing design concepts, derives occurring loads and elaborates on each component, as well as commonly used materials. Section 2.2 reviews current aircraft generations, which utilize discussed components and materials. The goal is to understand the importance of the evaluated structure in Chapter 3 and its arrangement in the structural wing design.

2.1. Structural Wing Design

The problem stated in Section 1.2, describes a general approach to optimizing stiffened plates, accordingly to certain constraints. To understand the validity of this substitution, this section briefly explains all main components and their specific arrangement in the overall wing structure.

Since the design of mechanical components generally depends on its exposure to outer and inner loads, Section 2.1.1 derives the loads on the structure under operational conditions. Section 2.1.2 breaks down the detailed design of the wing component by component and points out the importance to the wing structure to withstand the derived loads. At the end, in Section 2.1.3, commonly used materials are discussed and their influence on the design.

2.1.1. Wing Loads

This section discusses the occurring loads at the overall wing, due to aerodynamic and mechanical principles. The wing's purpose for the aircraft is to create the required up-force to lift the aircraft off the ground. Megson [33] describes it as a consequence of the resultant air flow, achieved due to the camber and angle of attack.

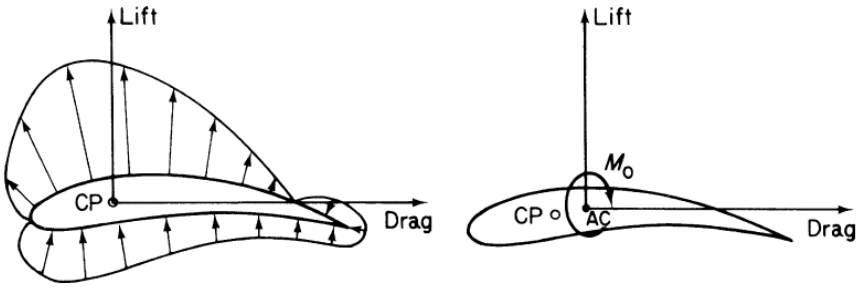

Figure 1 Pressure distribution over the wing and resultant forces [33].

This leads to a differential pressure distribution around the wing, as illustrated in Figure 1 and yields two primary forces. The resultant forces, lift and drag, act on the so called center of pressure (CP), which can vary chord-wise, depending on the local pressure distribution. The acting forces at the CP can be replaced with the respective forces at the aerodynamic center (AC), which has a fixed position and is independent of the pressure. The newly obtained moment is later discussed.

The resultant forces and moments deform the wing in a certain way. For easier comprehension, the wing is substituted with a cantilever model, where one side is fixed and the other free to move, following the explanation by Breuer [8] and illustrated in Figure 2. In correspondence to the present wing model, the root is fixed and the wing tip free to move. The distributed pressure around the wing's profile is substituted with a point force, acting upwards at the wings tip. This results in a bending deformation around the root, consequently, the upper side of the beam is compressed, while the lower half is under tension. Additionally, the upward force, perpendicular to the beam's surface, induces a transverse force along the normal axis. In regards to the discussion of the pressure distributions, the resultant lever arm between CP and AP leads to a torsional deformation, since the root is fixed and forces the beam to twist. When the beam is also deformed in the longitudinal axis, as it resembles a swept-back wing of commercial airliners, an additional lever arm

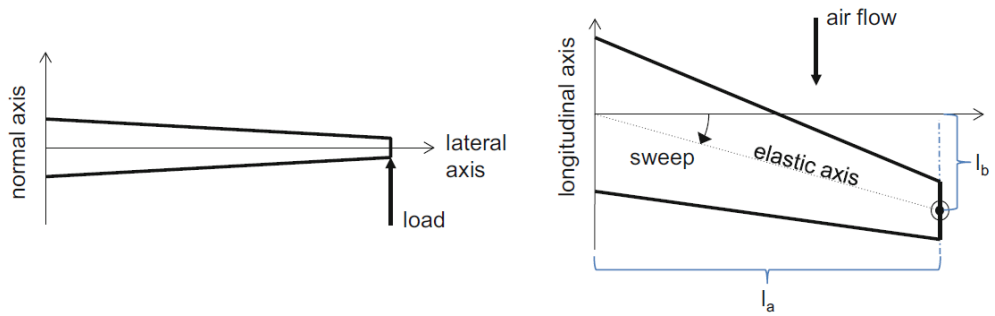

Figure 2 Beam model of aircraft wing and substituted force [8].

between the lateral axis and up-force is created, cf. right side of Figure 2, which also gives a torsional deformation.

Applying the simplified model to the present structural wing problem, three primary load cases are obtained, which are compression, torsion and transverse loads. For the scope of this thesis, these forces are sufficient for further discussion and the main reasons for the arrangement of the respective components, on which Section 2.1.2 elaborates.

2.1.2. Wing Components

Section 2.1.1 discussed certain loads to which the wing structure is subjected. Since these forces result from aerodynamic principles, most wings of operating aircraft, from general aviation and commercial airliners to military aircraft, share the same primary components to carry the resultant loads. The structural arrangement of the component is discussed in reference to Megson [33]. They might differ in wing configuration, quantity and strength of each component, but generally, the following parts are present: spars, ribs and skin, where the last is additionally stiffened by longitudinal stringers.

In most current aircraft wings, the spars are the biggest structural part of the wing and reach from the root to, or nearly to, the tip of the wing. For new aircraft generations with composite wings, however, this has changed, since the wing covers are made in one piece, as Section 2.2 shows. The number of spars depends on the mission profile of the respective aircraft. Commercial airliners generally have one front and one rear spar, to which numerous ribs are attached span-wise. The skin covers are usually riveted to the spars as well as the ribs and shape the cambered profile of the wing. Figure 3 shows a segment of the wing between to ribs (not shown) and defines the aforementioned components. In the following, the particular arrangement of each component is discussed.

To determine the role of the components as part of the overall wing structure, the previously discussed deformation shape, due to external forces is considered. It was stated, that the wing deforms upwards in combination with a wist around its lateral axis. The bending leads to a compression of the upper skin, thus is longitudinal compressed. This is resisted by the axial membrane stiffness of the wing, more specifically the upper wing cover. Since thin plates tend to buckle in compression, the skin is supported by stiffening elements, so called stringers. This divides the skin into smaller sections and increases both the membrane stiffness, due to distributing

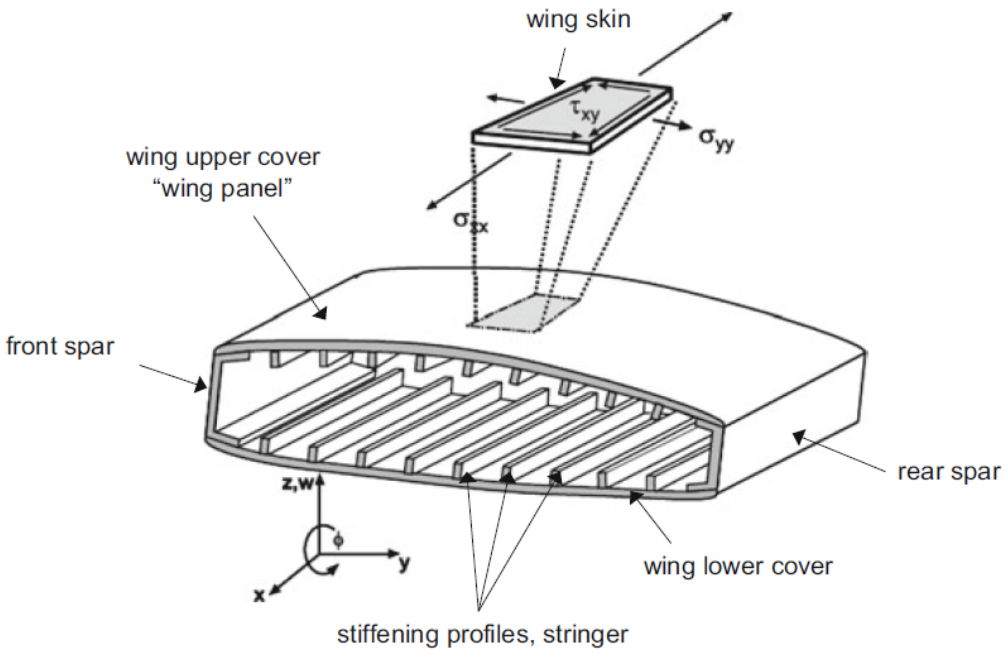

Figure 3 Torsion box of a structural wing and highlighted isolated area skin panel [8].

the compression force over the skin and stringer evenly, accordingly to Kassapoglou [26] and the buckling resistance, due to reducing the aspect ratio of the skin. The ribs additionally divide the skin span-wise into smaller sections, to further increase the buckling load, later discussed in Section 4.1.3. Furthermore, the skin is draped around the upper and lower edges of the ribs and attached to the front and rear spar, thus shapes the particular profile and guides the air-flow. This particular arrangement has another advantage, the so called torsional box, shown in Figure 3, which resists the twist, due to torsional deformation, by developing shear stresses.

In this section, the derived load cases from Section 2.1.1 were assigned to particular components of the structural wing. Accordingly to the stated problem in Section 1.2, the skin-stringer interaction is of higher interest, cf. isolated area Figure 3. As a consequence of the compression, the skin and stringer develop longitudinal in-plane stresses and due to torsion the skin develops additional shear stresses. Since the skin-stringer combination has a significant share of the entire wing, lightweight design are sought, specifically. Hence, these parts are highly eligible for the problem statement.

2.1.3. Materials

It was previously mentioned, that composite materials with directional dependent stiffness properties, i.e., orthotropic behavior, are specifically evaluated at DLR in

Brunswick. This section highlights certain differences between isotropic and orthotropic materials, for example aluminum and carbon fibre reinforced plastics, to understand the increasing complexity of structural design. The following information is based on the book Commercial Aircraft Composite Technology by Breuer [8].

Table 1 lists two common materials for aerospace applications, where aluminum 2024 has an isotropic behavior, while CFRP an orthotropic, indicated by the different E-moduli, parallel and perpendicular to fibre direction. The data shows, that CFRP has excellent strength properties with respect to its density. The tensile strength and E-Modulus considerably excel the metallic material values.

However, the main advantage of composite laminates, such as CFRP, is the directional varying stiffness. Laminates are generally build up of stacked layers, further discussed in Section 3.2, which enable the opportunity to tailored structures, i.e., adjust fibres to certain load paths, to obtain highly efficient designs. While for aluminum, the thickness must be locally increased to obtain the same results.

The downside of composites with respect to most isotropic materials, however, is the damage tolerance. Impact damages lead to de-lamination inside the structure, not visible without complex tools, which considerably decreases stiffness and might lead to a sudden failure, since it is a brittle material and tends to break unexpectedly. Aluminum has a much better damage tolerance and failure can often be predicted much earlier.

This section sought to point out differences between orthotropic and isotropic materials, in particular the directional properties. In reference to the problem statement, the possibility of varying the stacking and adjusting the stiffness to load paths, requires advanced optimization methods, which can handle a large amount of variables to obtain the most efficient design.

Table 1 Material properties of two particular materials[8], Einheiten fehlen

Material	Tensile Strength [MPa]	Density $\left[\mathrm{g/cm^3}\right]$	E-Modulus [GPa]	
			$E_\perp$	$E_\parallel$
AL 2024	420	2.78	69	
CFRP	1750 - 5000	1.75 - 196	240 - 500	5.7 - 15

2.2. State-of-the-art of Structural Wing Design

When it comes to detailed information about utilized technologies in new generation aircraft, manufacturers do not disclose too detailed information and making it not available to public. Consequently, this section gathers information about the structural wing design by evaluating published reports and conferences.

In August 2013, Bombardier announced in a press release [15] the maiden flight of its new commercial aircraft series the, CS100/CS300[1]. This is a good example, where a mix of well known aluminum material and new composite structures are combined, to achieve highly efficient vehicles. While the fuselage consists of metallic materials, the wing is fabricated from mostly composites. Bombardier published via press release [42] that the production of the wings uses preforms of dry fiber for skin and stringer at their new production site in Belfast. Gates [19], a Seattle Times[2] reporter, as well as Tyrrell [47] for aero-mag[3] reported, the manufacturing process of the wing structure is conducted in an autoclave process, where the resin is injected into the preformed stiffened panel and cures simultaneously. Hence, Bombardier follows an integrated stiffening concept, where the skin and stringer result in one large part. As stiffening elements, T-shaped stringers are taken. According to Gardiner [17], a writer for CompositeWorld[4], the same facility also produces the wing skins for Bombardier's new upcoming business aircraft Learjet 85, utilizing the same process.

Airbus decided on a slightly different approach to fabricating the wing structure of its A350. Fualdes [16], head of airframe certification at Airbus, hold a presentation at ICAS 2016[5] about the use of composite materials in their aircraft, on which the following information is based. The newest generation of long-range aircraft has with over 50% the highest amount of composites in its structure, compared to every other Airbus aircraft. Except from critical structural elements, such as door surroundings and high loaded frames, the primary structure is made completely from these. However, only the wing is of importance for the scope of this theis and as mentioned before, the manufacturing process differs from Bombardier's. While the Canadian manufacturer uses dry fibers, which are injected with resin, Airbus uses pre-impregnated material, so called prepregs. The skin panels are made in an automated tape laying (ATL) process on a solid mold, resembling the shape of the wing. After pre-curing the wing, "wet" T-stringer, i.e., not fully cured, are placed

[1] Administrated by Airbus since July 2018 [32] and renamed to A220-100/200
[2] `https://www.seattletimes.com`
[3] `https://www.aero-mag.com`
[4] `https://www.compositesworld.com`
[5] `http://www.icas2016.com/`

on the in-side of the panel and then co-bonded together during a second autoclave process.

As well as Airbus and Bombardier, Boeing offers a new generation aircraft, mostly made of composite materials, which had its first flight, announced in press release [29], in 2009. Accordingly to Reuters[6] [41], Boeing heavily counts on an international supply chain, where Mitsubishi Heavy Industry (MHI) is responsible for the wing covers. Boeing and MHI themselves, do not publish too much information about their structural design. However, according to the book Boeing 787 Dreamliner, written by Wagner and Norris [48], as well Norris [38] for NewsGlobal[7], the wing covers and stringers are fabricated using a co-bonding process. In contrast to Bombardier and Airbus, Boeing mainly uses a stiffener with I-cross-section as stringer. For Boeing, the newly developed composite design led to many delays, which also occurred due to the new wing design. Gates [18] published an article in correspondence with Boeing's engineers about problems with particular stringers around the wing root area, which are under too high loads and had to be redesigned. Since the aircraft was already in operation, an urgent fix was required and the problem solved, by cutting a U-shape into the web of each stringer, thus, the stresses could be better distributed and no de-lamination occurred anymore. Norris [39] published an article for Aviationweek[8], where an interesting picture of the wing root section is shown. The upper wing cover is, additionally to the already mentioned I-stringers, stiffened with Ω-stringers at the outer area of the string, which is not mentioned anywhere else.

However, this section reviewed the market of commercial airliners and showed the execution of structural wing design, particularly the skin-stringer concepts, by various manufactures. The arrangement coincides with the derived theory in Section 2.1 and shows, that different approaches are used. While Airbus and Bombardier stick to T-stiffeners, Boeing utilized I-stringer and possibly in combination with Ω-stringers.

[6] https://www.reuters.com
[7] https://www.flightglobal.com
[8] https://www.aviationweek.com

3. Analytical Formulation

Accordingly to the problem statement in Section 1.2 and the discussed structural wing components in Section 2.1, the skin-stringer interaction is of particular interest for this thesis and eligible for further analysis. The goal of this chapter is to derive an analytical formulation, which describes the stiffness properties of the stiffened panel. With a stiffness formulation, local stresses are determined, which develop due to deformation, as a result of external subjected loads and vice versa. To obtain the overall stiffness matrix, the single matrices of the skin and an equivalent-plate, i.e., the stiffener, are accordingly to Nemeth [37] and Kassapoglou [26], superimposed.

Therefore, Section 3.2 reviews the stiffness terms for orthotropic materials, which is the base for the equivalent-plate stiffness formulation, subsequently discussed in Section 3.3. This step is essential to conduct failure analyses and define optimization constraints, required for the optimization in Chapter 6. Since various papers use different denotations, depending on personnel preferences, Section 3.1 defines a mutual nomenclature for this thesis.

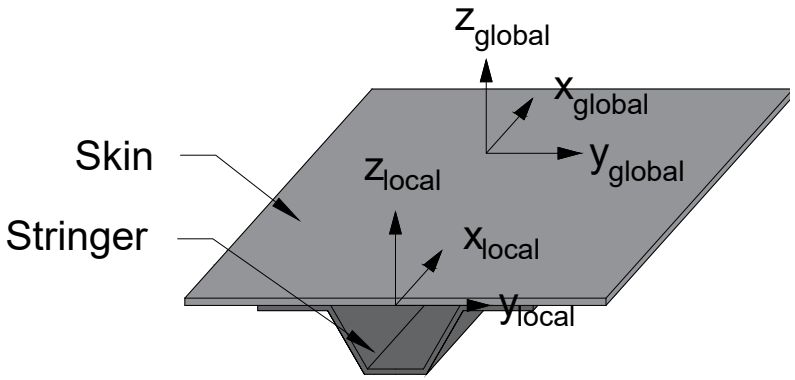

Figure 4 The skin stringer unit is shown with local and global coordination system, used for the analytical formulation.

3.1. Nomenclature

This section sets a common ground for the nomenclature in this thesis, as an addition to the list of symbols on Page III. Referring to a panel is done in two particular ways and distinguished chapter-wise. During the derivation of the analytical formulation in Section 3.3, thus the present chapter, the term panel denotes an isolated area, consisting of a plate, respectively skin, stiffened by one stringer of arbitrary shape, illustrated in Figure 4. The width of the panel corresponds to the stiffener spacing and the length is infinite, since it does not influence the stiffness terms, hence is of no concern at this point. In Chapter 4 and 5 the panel term is extended. It no longer refers to an isolated area, instead, it is a larger section of the skin braced by numerous longitudinal stiffeners and transverse ribs, cf. Figure 3 "wing panel". A single cross-section is then further annotated as isolated are of interest.

During this thesis, each member of the panel must be addressed separately. The plate, braced by stiffener, is in reference to aerospace applications and Section 2.1 referred to as skin. The stiffening part, so-called stringer, is further distinguished between open profiles, commonly named as the capital letters I and T, since the stiffener's cross-section mirrors the respective shape and between closed profiles, such as Ω, illustrated in Figure 5 . Each stiffener consists of single elements, which are denoted as foot, flange and web. The elements of the closed profile are further divided in a left and right representative and the flange is denoted as crown.

For the stiffener modeling, a coordinate system with its origin at the bottom of the skin is used and is the reference for the stiffener's height. However, the equivalent stiffness formulation in Section 3.3 uses a shared coordination system of skin and stiffener, which is for convenience located in the mid-plane of the skin.

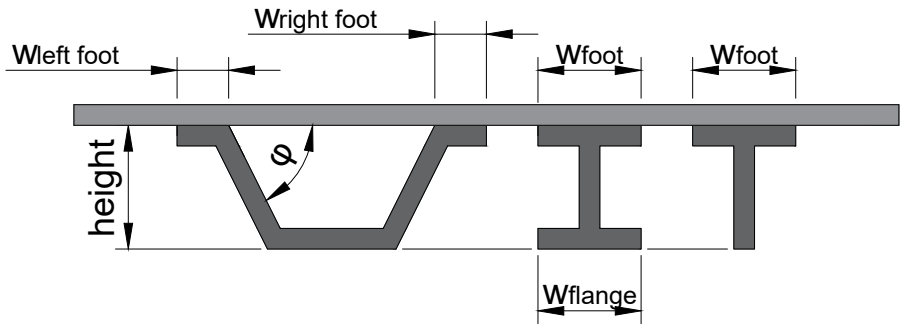

Figure 5 The illustrated figure shows a stiffened skin panel with three exemplary stiffening concepts and gives required notations for the analytical formulation.

3.2. Plate Stiffness

As previously stated, a stiffness formulation is used to determine in-plane stresses due to deformation of the respective plate. This section presents two common approaches to define the sought properties. In Section 3.2.1, the classical lamination theory (CLT) is reviewed, as it is the base for the equivalent-plate formulation in Section 3.3. Section 3.2.2 gives an alternative approach to determine the stiffness terms with so-called lamination parameters, which offers a well-suited method for gradient-based optimization, as discussed later.

3.2.1. Conventional Approach

A common approach to determine the stiffness matrix of orthotropic materials, in particular composites, is the classical lamination theory, first presented by Hahn and Tsai [22]. Composites are generally built up by stacking various layers, made of either the same or different material to a so-called laminate. To obtain the overall stiffness terms of the laminate, each layer is described by the $\boldsymbol{Q}$ matrix:

$$\boldsymbol{Q} = \begin{Bmatrix} Q_{11} & Q_{12} & 0 \\ Q_{12} & Q_{22} & 0 \\ 0 & 0 & Q_{66} \end{Bmatrix}, \tag{1}$$

where

$$Q_{11} = \frac{E_{11}^2}{E_{11} - \nu_{12} E_{22}}, \tag{2a}$$

$$Q_{12} = \frac{\nu_{12} E_{11} E_{22}}{E_{11} - \nu_{12}^2 E_{22}}, \tag{2b}$$

$$Q_{22} = \frac{E_{11} E_{22}}{E_{11} - \nu_{12}^2 E_{22}} \tag{2c}$$

and

$$Q_{66} = G_{12}. \tag{2d}$$

The material properties are given by the manufacturer, where E_{11} and E_{22} represent the Young's modulus of elasticity, parallel and perpendicular to the ply's fiber direction, respectively. G_{12} describes the shear modulus and ν is the Poisson's ratio. The local stiffness matrix in Equation (1) is independent from the distance of the reference plane to the mid-plane of the respective layer.

To obtain the actual stiffness properties of the stacked laminate, the local matrix of each layer is first transformed into the laminates coordination system, also referred

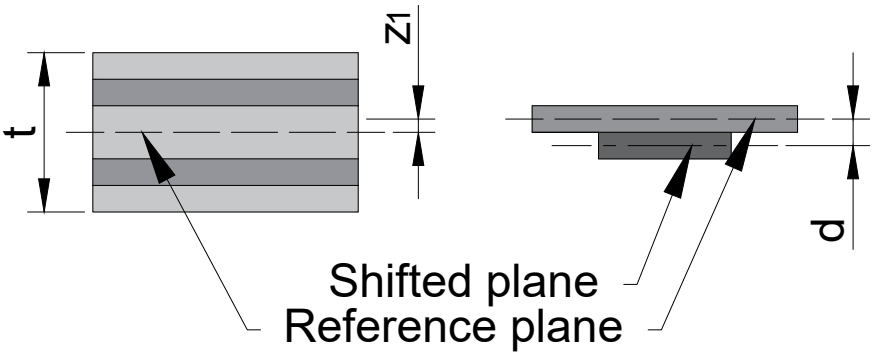

Figure 6 Illustrated is a stacked laminate with discrete thickness t on the left and the right figure shows the concept of a shifted laminate from the reference plane

to as global coordination system and denoted as $\overline{\boldsymbol{Q}}$. The transformation formulation is for brevity here omitted and discussed in Appendix A. The laminate's stiffness matrix, denoted as $\boldsymbol{ABD}$, reads:

$$\begin{Bmatrix} n_\mathrm{x} \\ n_\mathrm{x} \\ n_\mathrm{xy} \\ m_\mathrm{x} \\ m_\mathrm{x} \\ m_\mathrm{xy} \end{Bmatrix} = \begin{bmatrix} A_{11} & A_{12} & A_{13} & B_{11} & B_{12} & B_{13} \\ \vdots & A_{22} & A_{23} & \vdots & B_{22} & B_{23} \\ \mathrm{sym.} & \cdots & A_{33} & \mathrm{sym.} & \cdots & B_{33} \\ B_{11} & B_{12} & B_{13} & D_{11} & D_{12} & D_{13} \\ \vdots & B_{22} & B_{23} & \vdots & D_{22} & D_{23} \\ \mathrm{sym.} & \cdots & B_{33} & \mathrm{sym.} & \cdots & D_{33} \end{bmatrix} \begin{Bmatrix} \varepsilon_\mathrm{x} \\ \varepsilon_\mathrm{y} \\ \gamma\mathrm{xy} \\ \kappa_\mathrm{x} \\ \kappa_\mathrm{y} \\ \kappa_\mathrm{xy} \end{Bmatrix}, \tag{3}$$

where the vector on the left-hand side of Equation (3), contains the resultant internal in-plane and out-of-plane stresses, denoted as $\boldsymbol{n} = \{n_\mathrm{x}, n_\mathrm{y}, n_\mathrm{xy}\}$ and $\boldsymbol{m} = \{m_\mathrm{x}, m_\mathrm{x}, m_\mathrm{xy}\}$, respectively. They result from deformations of the laminate, which are denoted as $\boldsymbol{\varepsilon}^0 = \{\varepsilon_\mathrm{x}, \varepsilon_\mathrm{y}, \varepsilon_\mathrm{xy}\}$ and $\boldsymbol{\kappa} = \{\kappa_\mathrm{x}, \kappa_\mathrm{y}, \kappa_\mathrm{xy}\}$, where $\boldsymbol{\varepsilon}$ describes strains and $\boldsymbol{\kappa}$ the curvature of the laminate. The stiffness terms are defined as follows:

$$A_{ij} = \sum_{k=1}^{n} \left\{\overline{Q}_{ij}\right\}_n (z_k - z_{k-1}), \tag{4a}$$

$$B_{ij} = \frac{1}{2} \sum_{k=1}^{n} \left\{\overline{Q}_{ij}\right\}_n \left(z_k^2 - z_{k-1}^2\right), \tag{4b}$$

and

$$D_{ij} = \frac{1}{3} \sum_{k=1}^{n} \left\{\overline{Q}_{ij}\right\}_n \left(z_k^3 - z_{k-1}^3\right), \tag{4c}$$

where n is the number of layers and z the distance from the center-line of the laminate to the mid-plane of the respective layer, as shown in Figure 6. If a symmetric laminate is present, meaning the same lay-up above and below the center-line, as it is the case for most laminates in the aerospace applications, accordingly to Breuer

[8], the coupling matrix $\boldsymbol{B}$ equals 0.

The previously derived stiffness matrix in Equation (3) is only valid, when the reference plane equals the mid-plane of the laminate. However, in later operations, the laminate is shifted away from the reference plane. Thus, the distance, denoted as d, must be considered when deriving the stiffness terms. Mittelstedt and Becker [34] give the newly obtained and for brevity previously omitted formulation with:

$$N = \int_{z-\frac{h}{2}}^{z+\frac{h}{2}} \overline{\boldsymbol{Q}} \left(\varepsilon^0 + z\kappa^0\right) dz = \int_{\frac{h}{2}}^{\frac{h}{2}} \overline{\boldsymbol{Q}} \varepsilon^0 dz + \int_{\frac{h}{2}}^{\frac{h}{2}} \overline{\boldsymbol{Q}} \left(z + d\right) \kappa^0 dz, \tag{5}$$

which eventually leads to:

$$N = \mathbf{A}\varepsilon^0 + \left(\mathbf{B} + d\mathbf{A}\right) \kappa^0. \tag{6}$$

Analogously for moment stresses:

$$M = \int_{z-\frac{h}{2}}^{z+\frac{h}{2}} \mathbf{Q} \left(\varepsilon^0 + z\kappa^0\right) z dz = \int_{\frac{h}{2}}^{\frac{h}{2}} \mathbf{Q}\varepsilon^0 \left(z + d\right) dz + \int_{\frac{h}{2}}^{\frac{h}{2}} \mathbf{Q} \left(z + d\right)^2 \kappa^0 dz, \tag{7}$$

hence,

$$M = \left(\mathbf{B} + d\mathbf{A}\right) \varepsilon^0 + \left(\mathbf{D} + 2d\mathbf{B} + d^2\mathbf{A}\right) \kappa^0. \tag{8}$$

Transforming Equation (6) and (8) into matrix form gives the new espression with:

$$\begin{Bmatrix} \boldsymbol{n} \\ \boldsymbol{m} \end{Bmatrix} = \begin{bmatrix} \boldsymbol{A} & \boldsymbol{B} + d\boldsymbol{A} \\ \boldsymbol{B} + d\boldsymbol{A} & \boldsymbol{D} + 2d\boldsymbol{B} + d^2\boldsymbol{A} \end{bmatrix} \begin{Bmatrix} \boldsymbol{\varepsilon}^0 \\ \boldsymbol{\kappa} \end{Bmatrix}, \tag{9}$$

where for clarity, the matrix terms are shortened to the respective stiffness matrices $\boldsymbol{A}$, $\boldsymbol{B}$ and $\boldsymbol{D}$. In comparison to Equation (3) the membrane stiffness remains the same, since it is independent from the reference plane. The bending stiffness significantly increases due to the reliance on the aforementioned plane. More importantly, coupling terms are obtained, which commonly vanish, as previously stated. If the distance d is zero, the matrix complies with Equation (3).

Accordingly to the problem statement in Section 1.2 and the structural wing discussion in Section 2.1, the in-plane stresses of the skin can now be determined due to compression and shear deformation of the upper skin. To be mentioned, up to this point only the the skin is considered, the stiffening structure is accounted in Section 3.3.

3.2.2. Smeared Lamination Parameter Approach

Before defining the stringer's stiffness for the analytical formulation, an alternative approach for determining the laminate's stiffness properties is here discussed. It is utilized by various researchers who analyze composite materials with a gradient-based optimization method, such as Liu et al. [30] and Herencia et al. [23]. Accordingly to Dähne and Hühne [13], the stiffness matrices are defined in terms of 12 lamination parameters and 5 so-called material invariants. In addition with the laminate's thickness t, the stiffness terms are expresses as:

$$\begin{Bmatrix} A_{11}, B_{11}, B_{11} \\ A_{22}, B_{22}, D_{22} \\ A_{12}, B_{12}, D_{12} \\ A_{33}, B_{33}, D_{33} \\ A_{13}, B_{13}, D_{13} \\ A_{23}, B_{23}, D_{23} \end{Bmatrix} = \left[t, \frac{t^2}{4}, \frac{t^3}{12}\right] \begin{bmatrix} 1 & V_1^{\mathrm{A,B,D}} & V_2^{\mathrm{A,B,D}} & 0 & 0 \\ 1 & -V_1^{\mathrm{A,B,D}} & V_2^{\mathrm{A,B,D}} & 0 & 0 \\ 0 & 0 & -V_2^{\mathrm{A,B,D}} & 1 & 0 \\ 0 & 0 & -V_2^{\mathrm{A,B,D}} & 0 & 1 \\ 0 & V_3^{\mathrm{A,B,D}}/2 & V_4^{\mathrm{A,B,D}} & 0 & 0 \\ 0 & V_3^{\mathrm{A,B,D}}/2 & -V_4^{\mathrm{A,B,D}} & 0 & 0 \end{bmatrix} \begin{Bmatrix} U_1 \\ U_2 \\ U_3 \\ U_4 \\ U_5 \end{Bmatrix}, \tag{10}$$

where $U_{\{1,2,3,4,5\}}$ are the materials invariants and $V^{\mathrm{A,B,D}}_{\{1,2,3,4\}}$ the lamination parameters. The latter only depends on the distance from the reference plane to the particular ply, as well as on its rotation. The material properties have no influence to this point. Dähne and Hühne [13] define the lamination parameter as follows:

$$V^{\mathrm{A}}_{\{1,2,3,4\}} = \frac{1}{t}\sum_{k=1}^{N}\left(z_k - z_{k-1}\right)\left\{\cos\left(2\varphi_k\right), \cos\left(4\varphi_k\right), \sin\left(2\varphi_k\right), \sin\left(4\varphi_k\right)\right\}, \tag{11a}$$

$$V^{\mathrm{B}}_{\{1,2,3,4\}} = \frac{1}{t^2}\sum_{k=1}^{N}\left(z_k^2 - z_{k-1}^2\right)\left\{\cos\left(2\varphi_k\right), \cos\left(4\varphi_k\right), \sin\left(2\varphi_k\right), \sin\left(4\varphi_k\right)\right\}, \tag{11b}$$

and

$$V^{\mathrm{D}}_{\{1,2,3,4\}} = \frac{1}{t^3}\sum_{k=1}^{N}\left(z_k^3 - z_{k-1}^3\right)\left\{\cos\left(2\varphi_k\right), \cos\left(4\varphi_k\right), \sin\left(2\varphi_k\right), \sin\left(4\varphi_k\right)\right\}. \tag{11c}$$

As described by Wu et al. [51], a feasible domain is derived by constraining the laminate to certain aspect, hence a convex function for the lamination parameter is obtained. This thesis constraints the lamination parameter to design rules for aerospace applications, accordingly to Kassapoglou [26]. When symmetric laminates are present, IJsselmuiden et al. [24] state, that all $V^{\mathrm{B}}_{\{1,2,3,4\}}$ terms vanish. Additionally, only $\pm 45°$, $0°$ and $90°$ angles are present, consequently all $V_4^{\mathrm{A,B,D}}$ terms vanish, due to $\sin\left(4\varphi_k\right)$, in Equation (10), which is in compliance with Herencia et al. [23]. If furthermore, a balanced laminate is present, i.e., same amount of

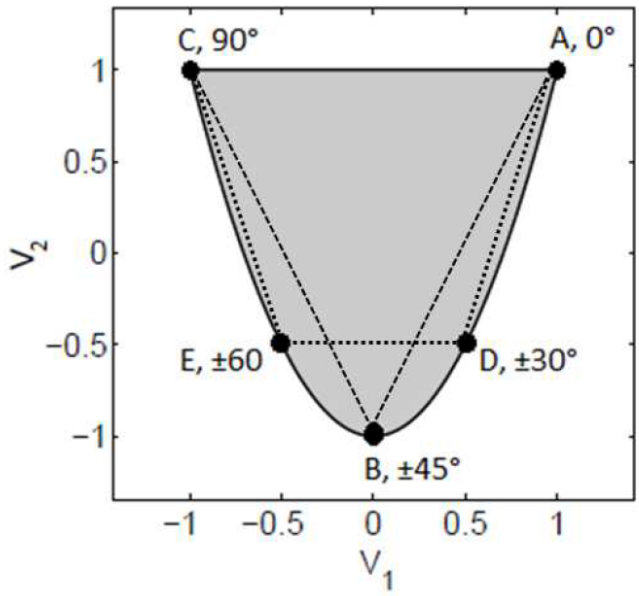

Figure 7 With the dependency between V_1 and V_2, a feasible domain can be defined, which predicts the required ply angles for the laminate [49].

positive and negative angles, Dähne and Hühne [13] set the $V^{\mathrm{A}}_{\{3,4\}}$ terms to 0. With the present assumptions, Werthen and Dähne [49] constrain the feasible domain of $V_1^{\mathrm{A,\,D}}$ and $V_2^{\mathrm{A,\,D}}$, accordingly to the area inside the triangle with corners A, B and C in Figure 7.

Since the lamination parameters do not account the material properties, the material invariants $U_{\{1,2,3,4,5\}}$ are defined in Equation (12), accordingly to Dähne and Hühne [13]. The stiffness terms Q_{ij} correspond to Equation (2) in Section 3.2.1.

$$U_1 = \frac{1}{8}\left(3Q_{11} + 3Q_{22} + 2Q_{12} + 4Q_{66}\right) \tag{12a}$$

$$U_2 = \frac{1}{2}\left(Q_{11} - Q_{22}\right) \tag{12b}$$

$$U_3 = \frac{1}{8}\left(Q_{11} + Q_{22} - 2Q_{12} - 4Q_{66}\right) \tag{12c}$$

$$U_4 = \frac{1}{8}\left(Q_{11} + Q_{22} + 6Q_{12} - 4Q_{66}\right) \tag{12d}$$

$$U_5 = \frac{1}{8}\left(Q_{11} + Q_{22} - 2Q_{12} + 4Q_{66}\right) \tag{12e}$$

In contrary to the classical lamination theory, the thickness of the laminate is not dependant of the discrete lay-up anymore. It can take any positive value, which allows to define the stiffness terms by continuous quantities and fixed material invariants, hence, this approach is well-suited for gradient-based approaches and utilized in Chapter 6.

3.3. Equivalent-Plate Formulation

In Section 3.2, the classical lamination theory was reviewed and the stiffness properties in form of the ***ABD*** matrix expressed. To process towards the objective of the problem statement, this section extends the obtained matrix by accounting the stiffening structure. Referring to Nemeth [37], the stiffener is smeared into and equivalent-stiffener layer with equivalent-stiffness formulation and then superimposed with the skin's local ***ABD*** matrix, hence:

$$\begin{bmatrix} (\boldsymbol{A})_{\text{panel}} & (\boldsymbol{B})_{\text{panel}} \\ (\boldsymbol{B})_{\text{panel}} & (\boldsymbol{D})_{\text{panel}} \end{bmatrix} = \begin{bmatrix} (\boldsymbol{A})_{\text{skin}} + (\boldsymbol{A})_{\text{stringer}} & (\boldsymbol{B})_{\text{skin}} + (\boldsymbol{B})_{\text{stringer}} \\ (\boldsymbol{B})_{\text{skin}} + (\boldsymbol{B})_{\text{stringer}} & (\boldsymbol{D})_{\text{skin}} + (\boldsymbol{D})_{\text{stringer}} \end{bmatrix}. \tag{13}$$

To allow this formulation, Nemeth [37] states, that the equivalent-stiffener layer undergoes the same deformation as the skin at any point, thus, both members share the same strains. The stiffness matrices for the skin are derived accordingly to the classical lamination theory and discussed in Section 3.2.1. The stringer's equivalent stiffness matrices are derived in the following sections, starting with the membrane stiffness in Section 3.3.1, then bending stiffness in Section 3.3.2 and finally in Section 3.3.3 the coupling between the previous two.

3.3.1. Equivalent Membrane Stiffness

The present section defines the membrane stiffness matrix, i.e., the resistance against deformation due to in-plane stresses, which reads, accordingly to Nemeth [37] and adjusted to the present case:

$$(\boldsymbol{A})_{\text{stringer}} = \begin{bmatrix} A_{11} & 0 & 0 \\ \vdots & A_{22} & 0 \\ \text{sym.} & \cdots & A_{33} \end{bmatrix} \tag{14}$$

In his publication, Nemeth [37] omits the transverse in-plane stiffness, i.e., the A_{22} term. However, the consideration in the present case is based on the derivation of the bending stiffness in Section 3.3.2 and the buckling analysis in Section 5.4.2, where the term is required to determine the corrected bending stiffness, elaborated on later more precisely. In the following, the single stiffness terms in Equation (14) are discussed.

Nemeth [37] derives the sought terms by partially integrating the axial in-plane stresses over the skin's and stringer's cross-section, where the stiffener is modeled

accordingly to Euler-Bernoulli and Timoshenko's first-order transverse-shear deformation beam theory, reviewed in Appendix A of his paper. This results in obtaining the local membrane stiffness of the stringer and eventually yields:

$$(A_{11})_{\text{stiffener}} = \frac{E_{\text{S}} A_{\text{S}}}{d_{\text{s}}}, \tag{15}$$

which is in compliance with Kassapoglou [26] and where A_{S} is the effective area and E_{S} the effective E-modulus of the stiffener, which further depends on the local moduli of the stiffener's elements.

The next required stiffness term in Equation (14) is A_{22}, the transverse membrane stiffness. Nemeth [37] and Kassapoglou [26] omit this term and state, that it is negligible for small foots. However, as previously mentioned, the present method accounts the foot. Mittelstedt and Becker [34] treat it as a shifted mid-plane from the reference plane, which, accordingly to Section 3.2 and considering the ratio of the foot to the spacing, reads:

$$(A_{22})_{\text{stringer}} = \frac{w_{\text{foot}}}{d_{\text{s}}} (A_{22})_{\text{foot}} , \tag{16}$$

where $(A_{22})_{\text{foot}}$ is the local stiffness term of the foot's laminate.

For A_{33} in Equation (12), the approach of Nemeth [37], analogously to A_{11} is followed, which eventually yields:

$$(A_{33})_{\text{stiffener}} = \frac{k_{\text{Y}}^{\text{S}} G_{\text{S}} A_{\text{S}}}{2 d_{\text{s}}}, \tag{17}$$

where G_{S} is the effective shear modulus and k_{Y}^{S} the in-plane shear correction factor. Equation (17) accounts in this form a shear resistance of the entire stringer. However, as seen in Figure 8, the shear stress in open profiles is nearly zero, when the load is introduced at the skin's edges, as discussed in Section 2.1, thus no shear flow through the stringer. Around the area, where the foot is attached to the skin on the contrary, the shear flow is distributed over the entire cross-section. This concludes, that only the foot develops a certain amount of shear stresses for open profiled cross-sections. Consequently, elements with no shear flow are omitted, in particular web and flanges. Furthermore, Nemeth [37] considers the shear correction factor k_{Y}^{S} in Equation (17), which is a consequence of the transverse-shear beam theory. It accounts the shear deformation when a constant shear flow through the cross-section is present. However, due to the different layers of ply angles and resin, it is not straight forward to predict. While for isotropic materials, various suggestions exist to determine the factor, which commonly varies around 8/9, according

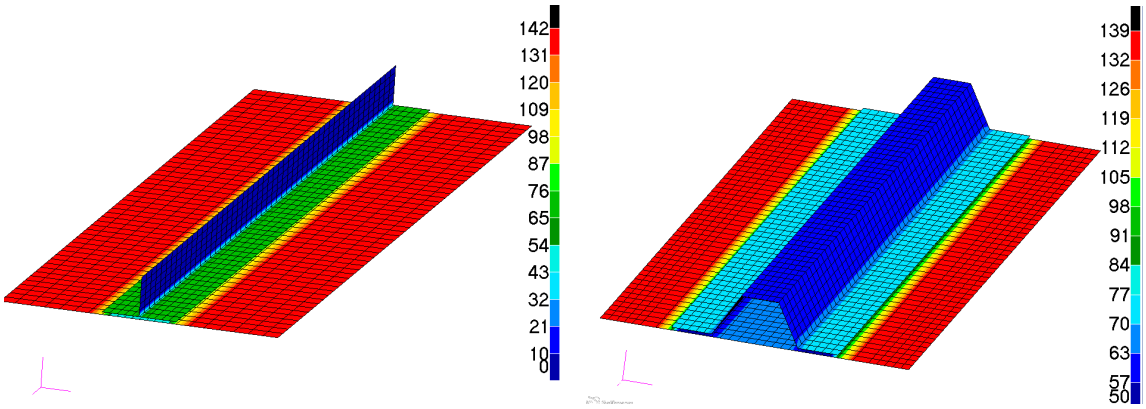

(a) The web of the open profile develops shear stress of under $1\,\mathrm{N\,mm^{-1}}$.

(b) The webs and crown of the closed profile develop constant shear stresses.

Figure 8 Shear stresses of a stiffened panel with either an open profile in (a) and a closed section in (b), where the shear load is induced around the edges of the skin. The spectrum's values are shown in $\mathrm{N\,mm^{-1}}$.

to a theoretical case study conducted by Stephen [45], for laminates it is less trivial. Gruttmann and Wagner [21] researched the behavior for curved panels by increasing the thickness, while Kulkarni [28] investigated on the behavior, when altering the ply angles. Madabhusi-Raman and Davalos [31] come to a similar result for laminated beams, an inconsistent shear correction factor. Furthermore, their researches are based on correction factors for a shear flow perpendicular to the mid-plane, while in the present case the shear load is induced in the horizontal layer. To avoid this inconvenience and source for unpredictable errors, Kassapoglou [26], Xu et al. [52] and Nemeth [37] simply set the shear deformation parameter to zero, which complies with various papers, mentioned in their publications.

To cover the foot's influence, while avoiding the shear correction factor, Collier [10] approaches the problem from a different view. He divides the skin-foot interaction into separate parts, the open span, as it is defined in Section 3.1, and treats skin-foot section as one laminate, where the width corresponds to the foot's width. The first sum of the denominator Equation (18) represents these sections.

$$(A_{33})_{\text{panel}} = \frac{d_{\text{s}}}{\sum\limits_{j=1}^{n} \frac{w_j}{(A_{33})_j} + \sum\limits_{i=1}^{n} \frac{w_i \cdot q_{cr}}{(A_{33})_j}}, \tag{18}$$

The second sum is only considered, when the stiffening structure has a closed profile, for example the Ω-stringer in Figure 8b. The shear flow is not only carried by the skin and foot anymore, it also goes through the profile, which leads to shear stresses in each element. The ratio of the shear flow through the closed profile, with respect

to the plate, is the so-called critical shear flow q_{cr} and given by Collier [10] with:

$$q_{\mathrm{cr}} = \frac{1}{1 + \frac{(A_{33})_{\mathrm{skin}}}{w_{\mathrm{cs}}} \left[\sum_{j=1}^{n} \frac{w_j}{(A_{33})_j} \right]}, \tag{19}$$

where w_{cs} is the span of skin inside the closed section and $(A_{33})_{\mathrm{skin}}$ the corresponding stiffness term of the skin. The sum in brackets represents each free element, for example webs and crown of the Ω-stringer. Equation (18) is not in full compliance with the stated formulation of the $\boldsymbol{A}$ matrix in Equation (14). It was initially stated, that all terms are simply superimposed, however, the discussion of the A_{33} showed, that the stiffness of stringer and skin are preferably determined as a unit and not separately, to avoid the shear correction factor.

In this section, the stiffness terms required for the equivalent-plate stiffness of the stringer were discussed and the $\boldsymbol{A}$ matrix adjusted for cross-sections either open or closed. For A_{33} an equivalent term was proposed by Collier [10], which describes the membrane shear for both skin and foot as a unit. Accordingly to Kassapoglou [26] and in compliance with Nemeth [37] and Collier [10], the other A_{ij} terms are omitted.

3.3.2. Equivalent Bending Stiffness

This section discusses, analogously to the previous derivation, the equivalent bending stiffness, represented by the $\boldsymbol{D}$ matrix. Section 2.1 pointed out the importance of stiffening elements for the buckling behavior of the skin itself, as well as of the entire skin panel, constraint by spars and ribs. The eccentric behavior of stiffening elements have the potential to increase the bending stiffness considerably, thus the critical buckling load, as later discussed in Section 4.1.3. The equivalent $\boldsymbol{D}$ matrix, discussed in the section yields in correspondence to Nemeth [37] and adjusted by the transverse bending stiffness:

$$(\boldsymbol{D})_{\mathrm{stringer}} = \begin{bmatrix} D_{11} & 0 & 0 \\ \vdots & D_{22} & 0 \\ \mathrm{sym.} & \cdots & D_{33} \end{bmatrix} \tag{20}$$

Analogously to the prior discussion, Nemeth [37] partially integrates the moment stress over the cross-section, which eventually yields:

$$(D_{11})_{\text{stringer}} = \frac{E_{\text{S}} I^{\text{S}}_{\text{YY}}}{d_{\text{s}}}. \tag{21}$$

I^{S}_{YY} is the stiffness weighted second moment of inertia of the effective cross-section and determined by general mechanical principles, found in common structural handbooks:

$$I^{\text{S}}_{\text{YY}} = \frac{\iint_{A_{\text{S}}} E_{\text{x}} Z^2 \, \mathrm{d}Y \, \mathrm{d}Z}{E_{\text{S}}}. \tag{22}$$

As the bending stiffness depends on the distance from a reference plane, the midplane of the skin is used as origin, since the coordination system of the panel must be taken, cf. Section 3.1. Accordingly to Nemeth [37] and Kassapoglou [26], the stiffening profile does not influence the plate's behavior in its transverse direction. However, due to the locally thickening effect of the foot, the bending stiffness around the x-axis can improve its behavior, especially with high foot widths, as later discussed in Section 4.1.3. Therefore, the foot's influence is, accordingly to Section 3.2 and Mittelstedt and Becker [34]:

$$(D_{22})_{\text{stringer}} = \frac{w_{\text{foot}}}{d_{\text{s}}} \left[(D_{22})_{\text{foot}} + z \, (B_{22})_{\text{foot}} + z^2 \, (A_{22})_{\text{foot}} \right], \tag{23}$$

Where $(D_{22})_{\text{foot}}$ and $(A_{22})_{\text{foot}}$ correspond to the local stiffness matrices of the foot's laminate.

Closed profiles, once again, have an extraordinary influence on the bending behavior. Figure 9 shows the deflection of a FE analysis, after subjecting the panel transverse bending loads. Each element of the stiffening structure deforms itself and contributes to the overall stiffness. The deflection shape corresponds with Mittel-

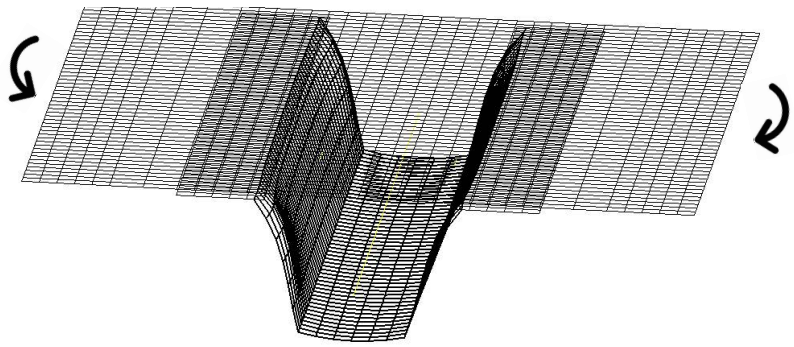

Figure 9 Shown is the local deformation shape of an Ω-stringer subjected to in-plane and moment loads. The skin deformation is omitted.

stedt and Schröder [36], who researched the buckling behavior of Ω-braced panels, subjected to transverse loads. To determine the extra stiffness, Collier [10] quantifies the elements, which gives:

$$(D_{22})_{\text{cell}} = \left(\frac{2(D_{22})_{\text{skin}} w_{\text{cs}}}{(D_{22}) w_{\text{web}}} + \frac{2(D_{22})_{\text{crown}} w_{\text{cs}}}{(D_{22})_{\text{skin}} w_{\text{foot}}} \right) \cdot \frac{2(D_{22})_{\text{skin}} w_{\text{cs}}}{d_s}, \tag{24}$$

where the subscript cell corresponds to the stiffness of the closed area only. Consequently one can say, that the Ω-stringer significantly increases the transverse bending behavior with $(D_{22})_{\text{stringer}} = (D_{33})_{\text{foot}} + (D_{33})_{\text{cell}}$.

The last undefined term of the equivalent bending stiffness in Equation (20) is D_{33}, the torsional deformation and the skin's resistance to camber. Following the approach by Nemeth [37], it reads:

$$(D_{33})_{\text{stringer}} = \frac{k_Y^{\text{S}} G_{\text{S}} A_{\text{S}} \overline{\overline{z}}}{2 d_{\text{s}}}, \tag{25}$$

where the variable $\overline{\overline{z}}$ is the shear stiffness weighted eccentricity. To avoid the reoccurring problem with the shear correction factor, the D_{33} term is discussed in detail. In Section 3.3.1 the shear flow through stiffening structures is discussed and stated, that a closed profile is capable of developing shear stresses. This behavior is also described through Bredt's formula for thin walled profiles, given by Wiedemann [50, Section 3.1.3.3]:

$$J = \frac{4 A_{\text{cell}}^2}{\oint \mathrm{d}s / t}, \tag{26a}$$

$$J = \frac{1}{3} \oint t^3 \mathrm{d}s, \tag{26b}$$

where Equation (26a) is for closed and Equation (26b) for open profiles, respectively. The variable A_{cell} is the enclosed area of the profile and approximated by Collier [10] with:

$$A_{\text{cell}} = \left(\frac{w_{\text{cs}} + w_{crown}}{2} \right) \cdot H_{\text{cell}}, \tag{27}$$

where, H_{cell} is the respective height of the closed section, measured from mid-plane of the skin to the center-line of the crown. Furthermore, $\mathrm{d}s$ is the perimeter of the closed section and must not be mistaken with the stiffener spacing. The variable t is the thickness of the respective element. Applying Equation (26a) to an arbitrary closed cross-section, Collier [10] defines the stiffness term of the cell with:

$$(D_{33})_{\text{cell}} = \frac{\dfrac{A^2}{d_s}}{G_{\text{f}} + \sum\limits_{j=1}^{n} \dfrac{w_j}{A_{33,j}}}, \tag{28}$$

where the sum inside the denominator represents each element of the stiffening structure, which is not associated with the skin, for example webs and the crown, whereby G_f accounts the connection between the stringer and the skin. Dependently on the manufacturing of the skin and stringer, Collier [10] distinguishes between two cases. First, the structure is not part of the panel and no shear flow is carried out. Second, a bonded connection, where the skin and the foot act as unit and allow shear flow through the closed profile. The two cases result in Equation (29a) and (29b), respectively.

$$G_\mathrm{f} = \frac{w_\mathrm{cs}}{(A_{33})_\mathrm{skin}} \qquad (29a) \qquad\qquad G_\mathrm{f} = \frac{w_\mathrm{foot}}{d_\mathrm{s}\,(A_{33})_\mathrm{skin\,+\,foot}} \qquad (29b)$$

For the present structure, an ideal connection is assumed, thus, Equation (29b) is taken. By comparing Equation (26a) and (26b), it is visible that the open profiles have much lower influence on the bending stiffness and are omitted by Nemeth [37] and Kassapoglou [26].

However, analogously to A_{33}, the foot's stiffness is considered with:

$$(D_{33})_\mathrm{foot} = \frac{w_\mathrm{foot}}{d_\mathrm{s}} \left[(D_{33})_\mathrm{foot} + 2z\,(B_{33})_\mathrm{foot} + z^2\,(A_{33})_\mathrm{foot} \right], \qquad (30)$$

which corresponds, once again, to a shifted laminate, given by Mittelstedt and Becker [34].

Consequently, one can say that three major terms influence the stringer's equivalent bending stiffness, the full stringer affects the $(D_{11})_\mathrm{stringer}$ term. $(D_{22})_\mathrm{panel}$ as well as the $(D_{33})_\mathrm{panel}$ are primarily influenced by a closed profile as well as by the foot. The other terms are, in accordance with the previously discussed papers by Nemeth [37], Collier [10] and Kassapoglou [26], omitted.

3.3.3. Equivalent Coupling

In reference to the classical lamination theory in Section 3.2, the $\boldsymbol{B}$ matrix results from unsymmetrical or shifted laminates, with respect to the reference plane. A stiffener acts similar, due to its one-sided eccentricity, thus yields coupling terms with:

$$(\boldsymbol{B})_\mathrm{stringer} = \begin{bmatrix} B_{11} & 0 & 0 \\ \vdots & B_{22} & 0 \\ \mathrm{sym.} & \cdots & B_{33} \end{bmatrix} \qquad (31)$$

The derivation of these coupling terms is based on the same principles as for the equivalent membrane and bending stiffness and results from integrating the stresses over the cross-section and reads:

$$(B_{11})_{\text{stiffener}} = \frac{\overline{z} E_{\text{S}} A_{\text{S}}}{d_{\text{S}}}. \tag{32}$$

It resembles the A_{11} term from Equation (15) with an additional variable z, which is the distance of the stiffness weighted centroid of the stiffener, with respect to the reference plane, hence:

$$\overline{z}_{\text{S}} = \frac{\iint_{A_{\text{S}}} E_{\text{x}} Z \, \mathrm{d}Y \, \mathrm{d}Z}{A_{\text{S}} E_{\text{S}}}. \tag{33}$$

Comparing it to the ***ABD*** matrix of the shifted laminate in Equation(9), the correlation of the aforementioned and eccentric stiffener can be seen.

Since the foot is considered for the membrane stiffness, it consequently must be accounted in the resultant coupling terms. Analogously to the previous discussion, it act as a shifted laminate, thus

$$(B_{22})_{\text{foot}} = \frac{w_{\text{foot}}}{d_{\text{s}}} \left[(B_{22})_{\text{foot}} + z \, (A_{22})_{\text{foot}} \right], \tag{34}$$

and

$$(B_{33})_{\text{foot}} = \frac{w_{\text{foot}}}{d_{\text{s}}} \left[(B_{33})_{\text{foot}} + z \, (A_{33})_{\text{foot}} \right]. \tag{35}$$

The B_{33} term for the closed profile is determined accordingly to Collier [10] and based on Bredt's formula for torque, given by Wiedemann [50, Section 3.1.3.3]. By considering the relation of torque to the bending-twisting moment, as well as the shear flow through the panel Collier [10] defines B_{33} as:

$$(B_{33})_{\text{cell}} = A_{\text{cell}} q_{\text{cr}} \frac{(A_{33})_{\text{panel}}}{d_{\text{s}}}, \tag{36}$$

where q_{cr} is the critical shear load, defined in Equation (19) and A_{cell} is the enclosed area of the profile, determined accordingly to Equation (27). $(A_{33})_{\text{panel}}$ corresponds to the stiffness term of the panel, thus skin, foot and potentially the closed cell in Equation (18).

Consequently, one can say that three major terms influence the panel's stiffness, the full stringer affects the $(B_{11})_{\text{panel}}$ term, the foot the $(B_{22})_{\text{panel}}$ term, and the $(B_{33})_{\text{panel}}$ term is primarily influenced by a closed profile as well as by the foot. The other terms are, in accordance with the previously discussed papers by Nemeth [37], Collier [10] and Kassapoglou [26], omitted.

After pointing out eligible components for the previously conducted analysis in Chapter 2, this chapter was an important step towards solving the problem statement. This chapter discussed the derivation of an analytical formulation, to define equivalent stiffness properties of the plate-stringer combination to determine internal stress, due to deformation and vice versa. To verify the present formulation a thorough validation is conducted in Chapter 5.

4. Implementation

The derived analytical formulation in Chapter 3 is valid for plates stiffened by arbitrary cross-sections with either open or closed profiles. As validation of newly implemented concepts into the base code requires thorough verification to ensure accurate results, only certain concepts are taken into consideration.

Therefore, Section 4.1 discusses common stiffening solutions for aerospace structures, accordingly to Kassapoglou [26] and the HSB [1]. To make a proper choice of eligible cross-sections, which allow the validation of different sources of errors, while being feasible for the actual structural wing design, Section 4.1 subsequently evaluates the predefined set with respect to various criteria. After a certain choice is made, Section 4.2 elaborates on the implementation into the code.

4.1. Evaluation of Stiffening Concepts

Section 2.1 pointed out the importance of stiffening structures, in particular of the skin cover, for the overall wing design. The market overview in Section 2.2 showed, that this can be done in various ways. Referring to Kassapoglou [26] and HSB [1], Figure 10 illustrates a predefined selection of common stiffening structures. To reduce the broad set and pick eligible concepts, this section analyzes typical criteria to consider their feasibility for the validation in Chapter 5.

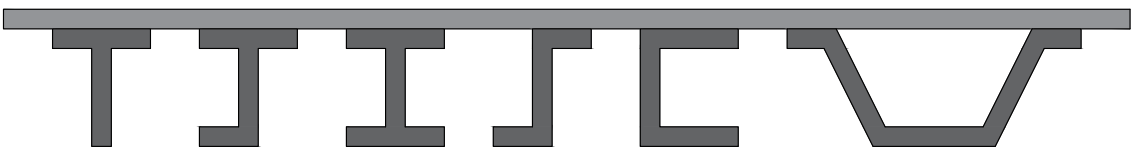

Figure 10 An overview of typical stiffening cross-sections, which are considered in this thesis and denoted as T, J, I, Z, C and Ω (from left to right).

4.1.1. Stiffness Properties

The stiffness property of the stringer, particularly in its x-direction, is a highly important factor for the design of the entire wing. As introduced in Section 2.1, the design differs from manufacturer to manufacturer and is usually referred to certain design philosophies. A primary influence on the stringer's stiffness is the second moment of inertia, denoted as I_x and reads:

$$I_\mathrm{x} = \iint_A y^2 \mathrm{d}x\mathrm{d}y, \tag{37}$$

where y is the distance from the reference point to the centroid of each element. Considering this equation, it can be concluded, that stiffening structures with elements far away from the reference plane have a high stiffness. For example an I-cross-section has most likely a higher bending stiffness than a T-stiffener. The HSB [1, 01712-01 - 01728-01] lists predetermined values for various cross-sections, which comes to the same conclusion. Whether the flange is centered, or attached by one corner, referring to I- and J-stiffeners, respectively, is irrelevant at this point.

4.1.2. Torsional Rigidity

While deriving the stiffness terms for the equivalent bending matrix in Section 3.3.2, the significant difference between open and closed stiffening profiles was discussed. It showed, that closed profiles specifically increase the panel's resistance ability to camber, due to developing shear stresses in its elements. To further discuss the influence, Bredt's formula for torsional stiffness is reviewed, as it is given in the HSB [1, 01610-05, Issue B]:

$$I_\mathrm{t} = \frac{4A_\mathrm{m}^2 t}{U_\mathrm{m}} \tag{38a}$$

$$I_\mathrm{t} = \frac{\eta}{3} t^3 U_\mathrm{m}, \tag{38b}$$

Besides the slightly different notation, it takes almost the same form as before. The HSB [1] accounts an additional efficiency factor for open cross-sections, denoted as η. Table 2 lists respective factors for some profiles. It shows, that even though no shear flow is achieved, a difference of $\approx 30\%$ between L- and I-shaped stiffeners is

Table 2 Sectional factors for open cross-section [1]

Section	L	C	T	I
η	0.99	1.12	1.12	1.31

obtained. However, when seeking high torsional stiffness, the Ω stiffener is still the best choice with its closed profile, thus, ability to develop shear stresses. For open structures, the slightly extra torsional stiffness must be gauged whether it is worth the more complex structure or not.

4.1.3. Buckling Behavior

The previous two sections evaluated the stiffness performance of the stringer on its own. However, as stated in Section 2.1, the panel is primarily subjected to compression and shear loads and the skin, or rather the skin-stringer assembly interact as unit. Consequently, critical buckling cases must be evaluated together, since the cross-section can significantly alter the panel's behavior. As analyzed in various papers, such as Bisagni and Vesconi [6] and Coburn et al. [9], the compression of stiffened plates leads to particular buckling modes, illustrated in Figure 11. The first mode discussed in this section, is the global buckling of a stiffened section, braced by repetitive stiffening elements and constraint, corresponding to the structural wing design in Section 2.1, by spars and ribs, cf. Figure 11a. Further buckling modes particularly affect local elements of the panel, for example the skin between the stiffeners or the web on its own, cf. Figure 11b. Both cases, global as well as local buckling are considered as total failure of the structure and are discussed below.

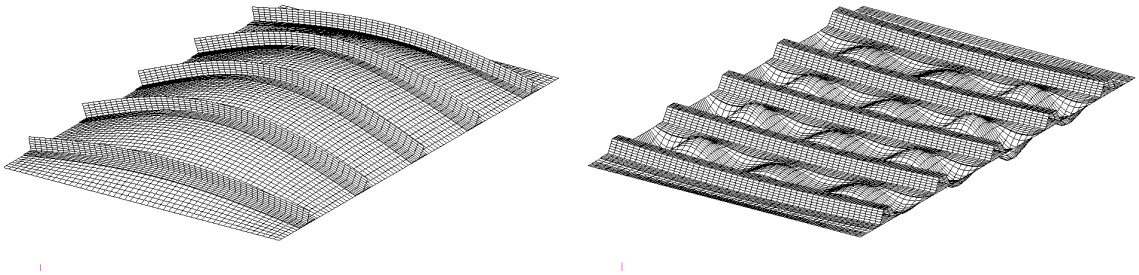

(a) Global buckling of panel. **(b)** Local buckling of spacing span.

Figure 11 The illustrated figures show two particular buckling modes, when the panel is subjected to an axial compression load. The figure in (a) resembles global buckling of the stiffened panel, while (b) resembles the local buckling between the stringers.

Global Buckling

As mentioned, the first evaluated failure mode is the global buckling of the panel. Therefore, the HSB [1] gives an expression for compression with:

$$n_{\mathrm{x,\ cr,\ comp}} = k_{\mathrm{x,\ comp}} \left(\frac{\pi}{b}\right)^2 \sqrt{\tilde{D}_{11}\tilde{D}_{22}} \tag{39}$$

and for shear with:

$$n_{\mathrm{x,\ cr,\ shear}} = k_{\mathrm{x,\ shear}} \left(\frac{\pi}{b}\right)^2 \sqrt[4]{D_{11}D_{22}^3}, \tag{40}$$

where $k_{\mathrm{x,}}$ is the respective buckling coefficient, discussed later. The stiffness terms $\tilde{D}_{11}$ and $\tilde{D}_{22}$ define the bending resistance of the evaluated element. For the present case, they are determined by the equivalent-plate stiffness, derived in Chapter 3. The given Equations (39) and (40), however, are derived for symmetric laminates, but since the eccentric stiffeners yield coupling terms, an asymmetrical behavior is obtained. Therefore, the HSB [1] provides a corrected plate stiffness formulation with:

$$\tilde{\boldsymbol{D}} = (\boldsymbol{D})_{\mathrm{panel}} - (\boldsymbol{B})_{\mathrm{panel}}^{\mathrm{T}} \cdot (\boldsymbol{A})_{\mathrm{panel}}^{-1} \cdot (\boldsymbol{B})_{\mathrm{panel}}\,, \tag{41}$$

which is indicated by the tilde above the terms. However, the corrected bending stiffness is not specifically mentioned for the shear buckling formulation, but as later analysis shows, Equation (40) shows accurate results for asymmetric stiffness matrices, thus $\boldsymbol{D} \equiv \tilde{\boldsymbol{D}}$ is assumed.

The buckling coefficient in Equation (39) corresponds to the boundary conditions of the respective element. Referring to Section 2.1, the skin is constrained by ribs and spars and according to Megson [33] and various further researchers, such as Barkanov et al. [4], simple supported boundary conditions can be assumed for the global buckling mode. Hence, the coefficient reads, accordingly to the HSB [1]:

$$k_{\mathrm{x,\ comp}} = h\left(\overline{\alpha}\right) + q \cdot \beta \tag{42}$$

with

$$\alpha = \frac{a}{b}\sqrt[4]{\frac{\tilde{D}_{22}}{\tilde{D}_{11}}} \tag{43a}$$

$$\beta = \frac{\tilde{D}_{12} + 2\tilde{D}_{33}}{\sqrt{\tilde{D}_{11}\tilde{D}_{22}}}, \tag{43b}$$

where α is the effective aspect ratio and β is Seydel's orthotropy. The variable q takes a fixed value of 2 for simply supported boundary conditions, cf. HSB [1]. The shear buckling coefficient is given in a plot in the HSB [1] and approximated by

Dähne and Hühne [13] with:

$$k_{\text{x, shear}} = a_1 \cdot \alpha^2 + 0.3 \cdot \alpha + a_2, \tag{44}$$

where:

$$a_1 = 2.6657 \cdot \beta + 1.0237 \tag{45a}$$

$$a_2 = -0.1667 \cdot \beta^2 + 2.2333 \cdot \beta + 3.3. \tag{45b}$$

With the given Equations (39) and (40), the critical global buckling loads are determined.

Local Buckling

The second analyzed buckling mode is exemplary illustrated in Figure 11b, where the spacing span of an Ω-braced panel buckles locally. The stiffening elements remain nearly straight in comparison to Figure 11a. Figure 12 shows further sections of the stiffened panel, which must be analyzed for critical buckling loads. The colored borders enclose the defined sections and the annotations refer to either the respective width of the element or its boundary conditions. In the following, the critical areas are discussed in more detail. Therefore, Kassapoglou [26] introduced the terms no-edge-free (NEF) and one-edge-free (OEF), which correspond to the simple support all around the respective element and to three sides simply supported and edge free to move, respectively. In Figure 12, the web of the T-stringer and the flanges of the I-stringer, cf. green areas, corresponds to OEF. All elements of an Ω-stringer, the web of I-stringers, as well as the open and spacing span correspond to NEF. The characteristic of the spacing span is different to the other cases, since the reference plane remains in the center of the skin, coupling terms are obtained, due to smearing

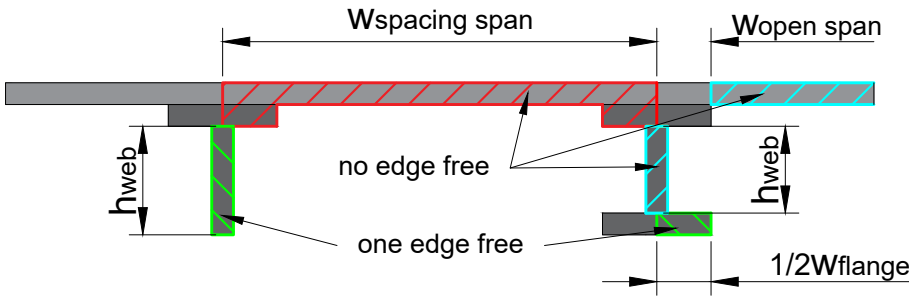

Figure 12 Required sections are shown, which must be analyzed to buckling with the respective width and boundary conditions. NOF refers to a simple support all around the element, while for OEF three sides are supported and one free to move.

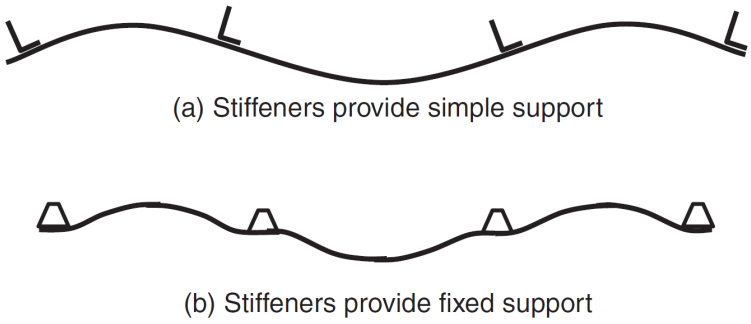

Figure 13 Local buckling shape of spacing span with two particular support assumptions, where (a) is obtained for open and (b) for closed profiles [26].

the foot into the skin, analogously to Section 3.3.

The spacing span between the stringers is further discussed now, therefore, Figure 13 shows an oversimplification of Figure 11b, to discuss the present boundary conditions. Particularly (a) is an expected deformation shape, according to Kassapoglou [26] and Coburn et al. [9]. The stiffening cross-section rotates around its own axis, thus, resembles a simply support for the inner span. This behavior also corresponds to the HSB [1] and Wiedemann [50], where the support is located at the root of the web, despite of the foot's geometry. Stamatelos et al. [44] enhances this support, by assuming an elastic behavior of the beam, i.e., restrains the rotation as a function of the stringer's stiffness. However, following the approach of most previously mentioned papers, a simple support is an eligible assumptions for open profiles and yields accurate results in later calculations..

Accounting Figure 13b, however, closed profiles acts differently. Due to its high torsional stiffness, as discussed in Section 4.1.2, the stringer prevents rotation of the spacing span at the edges, thus, accordingly to Kassapoglou [26], the Ω-stringer resembles a rigid support. However, as good as these assumptions seem, the actual support is more complex. To apply fixed boundary conditions, the stringer has to be infinite stiff and must not deform. Mittelstedt and Beerhorst [35] analyzed the boundary conditions, given by an arbitrary Ω-stringer in more detail. In particular, they derived an elastic spring coefficient, which is dependant on the local stiffness of the stringer's elements and how it influences the actual boundary conditions, i.e., proposed a support condition between simple and fixed. The newly obtained critical buckling load reads:

$$N_{\mathrm{cr}} = \frac{8\pi^2}{w_{\mathrm{ss}}^2}\left(\sqrt{\frac{\tau_1}{\tau_2}}\sqrt{D_{11}D_{22}} + \frac{\tau_3}{\tau_2}\left(D_{12}+2D_{66}\right)\right), \tag{46}$$

where

$$\tau_1 = 3D_{11}^2\pi^2 + 20kw_{\text{ss}}D_{22} + 3k^2w_{\text{ss}}^2 \tag{47a}$$

$$\tau_2 = 48D_{11}^2\pi^2 + 128kw_{\text{ss}}D_{22} + 9k^2w_{\text{ss}}^2 \tag{47b}$$

$$\tau_3 = 12D_{11}^2\pi^2 + 32kw_{\text{ss}}D_{22} + 3k^2w_{\text{ss}}^2 \tag{47c}$$

The elastic spring coefficient, denoted as k in Equation (47), accounts the stiffness properties of each element of the closed profile and their interaction. For clarity, Appendix B gives the proper derivation. The applicability of their work is discussed later in Section 5.4.2.

To cover each stiffening concept and simultaneously ensure safe results, a conservative approach is firstly used to determine the critical buckling of the spacing span. Therefore, Equation (39) is taken, to determine the critical load of simply supported laminates. The stiffness terms depend on the respective stiffening cross-section. For blade stiffeners for example, when no foot is present, only the plate's properties are considered, hence, $\tilde{\boldsymbol{D}} \equiv (\boldsymbol{D})_{\text{skin}}$. Otherwise, when the stiffener has a foot, the additional stiffness properties are smeared into the plate, accordingly to Chapter 3. Due to the resulting asymmetry of the equivalent-plate formulation, the corrected $\tilde{\boldsymbol{D}}$ matrix, accordingly to Equation (41), must be taken. Consequently, the stiffness matrix for the buckling analysis of the spacing span reads $\tilde{\boldsymbol{D}} \equiv \left(\tilde{\boldsymbol{D}}\right)_{\text{skin + foot}}$.

Referring to Section 2.1, the compression load is equally distributed over the skin and stringer. Consequently, each element of the stiffener must be verified in terms of local buckling. As previously discussed, Kassapoglou [26] differs between one-edge-free and no-edge-free. The importance of this can be expressed with the buckling coefficient, as given in the HSB [1] for NEF:

$$k_{\text{x}} = h\left(\overline{\alpha}\right) + q \cdot \beta \tag{42, reviewed}$$

and analgously for OEF:

$$k_{\text{x}} = h\left(\overline{\alpha}\right) + q \cdot \beta + r \cdot \eta, \tag{48}$$

The HSB [1] gives various plots to determine the so-called auxiliary function $h\left(\overline{\alpha}\right)$, which yields to an approximated value of 2 and 1 for NEF and OEF, respectively. For the latter and accordingly to the HSB [1], Seydel's orthotropy parameter vanishes,

Table 3 Respective plate widths and boundary conditions for global and local buckling analysis. S = simple, C = clamped, F = free edge. Detailed dimensions stated in Section 3.1.

Element	Width	Support
Global span	Panel width	SSSS
Spacing span	Spacing for open cross-sections and spacing span for closed	SSSS
Open span	The span between the stringer's foot	SCSC
Web, unsupported	Height of web	SSSF
Web, supported	Height of web	SSSS
Flange	Width of flange measured from web to free edge	SSSF
Crown	Width of crown	SSSS

due to $q = 0$. The parameter $r = 0.608$ and η is defined as:

$$\eta = \frac{2 \cdot \tilde{D}_{33}}{\sqrt{\tilde{D}_{11} \cdot \tilde{D}_{22}}}. \tag{49}$$

Comparing the two buckling coefficients, one can conclude that NEF has a significantly higher critical buckling because of a twice as high auxiliary function as well as due to considering β. Applying this to the present set of stiffening concepts, following can be established. Stiffeners with a flange yield much higher local critical loads, due to the NEF condition of the web. Furthermore, a flange width is taken from the web to free end, cf. Figure 12. Thus, the aspect ratio, cf. Equation (43a), is larger, consequently higher critical buckling loads. The Ω-stringer only has NEF elements, hence, highest local buckling load. Table 3 list all elements, which must be evaluated during the buckling analyses with respective widths and boundary conditions.

4.1.4. Fabrication and Manufacturing

The previous discussion evaluated the stiffening concepts in terms of stiffness properties and failure criteria for the panel. However, the fabrication process can have a significant influence on the manufacturer's choice, since production must be feasible and, eventually, profitable. Therefore, this section gives a broad overview of the potential influence of fabrication processes for the stiffening concept.

Kako et al. [25] held a presentation at CFK Valley Stade Convention[1] in 2013 about the production process of the A350XWB upper wing cover. He states, that approx-

[1] `https://cfk-valley.com`

imately 300 m of T-stiffeners are required per upper wing cover. Gillessen [20] from the Composite Technology Center in Stade, discussed at Innovation Day in 2013 the feasibility of a composite wing for the A320. With a desired production rate of 60 aircraft per month, 21 600 m of stringers are required just for the wings, additionally 6000 m for the vertical tail.

The high amount of stiffening elements requires efficient and profitable solutions. Gillessen [20] mentions specifically the pultrusion resin transfer molding (PRTM) process, which allows a continuous production of all previously mentioned concepts. Breuer [8] additionally mentions the feasibility of producing I-shaped stiffeners, which are cut horizontally, hence, twice as much T-profiles are obtained. Another way to produce continuous profiles, is Automated Stiffener Forming (ATF), patented by Orbital ATK [40], who produces the Ω-stringer for the fuselage of the A350XWB.

Besides the production of stiffening elements, the handling and fabricating process is also very important. Breuer [8] thoroughly discussed various options, but for the scope of this section only two ways are briefly mentioned, referring to Section 2.2. Airbus and Boeing use a co-bonding process for their wings, i.e, "wet" stringers are placed on the pre-cured skin and during an autoclave process bonded together. This allows the use of PRTM production of the stringers, thus high output. Bombardier, in contrary, uses a co-curing process, i.e., stringers and skin cure simultaneously. Accordingly to Breuer [8], it yields better laminate quality for the overall structure, however, the tooling required for this process is more cost consuming and production cycles need longer.

This section comprehensively showed, that certain ways are feasible to manufacture the skin-stringer cover and not always depend on highest quality, it also must fit into the production cycle of the overall aircraft to be profitable.

4.1.5. Selection Assessment

The previous sections discussed how the cross-sectional design influences the stringer's properties and which effect it has on the overall panel. In this section, the criteria are applied to the pre-defined set of stiffening cross-sections, cf. introduction of Chapter 4 and illustrated in Figure 10, to choose a particular selection for the implementation. The structures are also chosen with respect to the possibility of investigating sources of potential errors.

The discussion of stiffness properties in Chapter 3 showed, that the stiffener's influ-

ence on the shear stiffness is often omitted, such as by Nemeth [37] and Kassapoglou [26]. However, the preliminary FE-analysis showed, that the foot can definitely have an influence. Therefore, a T-cross-section is a feasible choice to determine the influence, especially in regards to Dähne and Hühne [14], who showed that a plain blade stiffener yields low errors. Furthermore, the overall stringer dimensions are kept small, further discussed in Section 5.1.1, to obtain a low stiffened panel to analyze the global buckling behavior. Additionally, since it is used for current generation aircraft, as Section 2.2 showed, it is a reasonable choice.

As an extension for the T-stringer, a flange gives a high overall bending strength of the panel and most likely tends to a post-buckling behavior, ie.e. the skin between the stiffener buckles first. To achieve this, various cross-sections are present, such as I, J, Z and C. However, the market research in Section 2.2 showed, the I-stiffener is used by Boeing to stiffen their composite wings. Accordingly to Kassapoglou [26], stiffeners with one-sided, such as Z and C should be avoided, since they lead to instabilities due to voids at the edge of the web during manufacturing. Furthermore, the centered flange will most probably lead to a symmetric failure shape, which is at this point desirable to investigate the flange's influence. Hence, the I-stringer is the second choice to be implemented into the code.

While deriving the analytical formulation in Section 3.3, the difference between open and closed profiles was thoroughly discussed. It was concluded, that closed structures most likely excel every other cross-section in terms of stiffness properties. Therefore, a closed profile, such as the Ω-stiffener is of high interest as third geometry. Despite the more complex geometry, Airbus and Boeing utilizes the stiffener for certain areas. While Boeing potentially uses Ω-stringer in addition to it's I-stiffeners for the wing, Airbus utilizes it to stiffen the fuselage in longitudinal direction.

This section analyzed various stiffening concepts to certain selection criteria, particularly failure modes and stiffness properties. The assessment concluded, that three stiffening cross-sections are eligible for the implementation as well as for the validation. Therefore, the derived analytical formulation in Chapter 3 is applied to the T-, I- and Ω-concepts and the resultant equations are listed in Appendix D to E.

4.2. Code Implementation

To this point of the thesis, an analytical formulation to define stiffness properties is derived in Chapter 3 and applied to three eligible concepts, where the resultant

equations are listed in Appendix C to E. This section describes the implementation of the stiffening concepts into the optimization environment. The objective is to seek minimal computation effort during the optimization to reduce run time. Therefore, the code is structured into three primary classes, the first class defines the stiffening models and determines the stringer's ***ABD*** matrix, while the second defines the skin's properties, accordingly to the classical lamination theory in Section 3.2. The third class finally defines the equivalent-plate stiffness matrix and executes the failure analysis of the panel.

The stiffening structure inside the first class, is modeled by defining single instances of flat laminates and subsequently combining them, until the desired cross-section is obtained. To specify this process, Figure 14a shows an exemplary stiffener, modeled with five instances. The filleted corners are deliberately omitted, since they are not considered in the analytical formulation and which this gives an important advantage. The complex structure is reduced to single elements, i.e., laminates, whose properties can be specifically described. However, to obtain the desired cross-section, each element is represented by a unique instance with particular rotation and coordinates, as shown in Figure 14b. As a reference for the origin of the coordination system the stiffeners local coordination system is taken. When deriving the analytical formulation, an offset is applied to obtain stiffness properties with respect to reference plane. In Figure 14c the element is further isolated to discuss its properties. This instance is defined by its length and thickness, which result from the pre-defined stringer geometry and laminate lay-up, respectively. Consequently, the stiffener's equivalent ***ABD*** matrix is defined by local element with specific properties and their arrangement in the stiffener's coordination system.

This process enables future extensions of newly integratable concepts. Since the

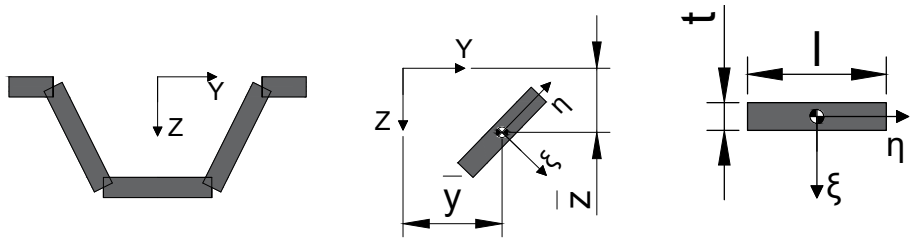

(a) Modeled stiffener **(b)** Beam location **(c)** Beam element

Figure 14 The three figures show the process of modeling a beam inside the optimization environment. In (a), an exemplary stiffener is modeled by an arrangement of five beam elements which are defined by a single element which is located inside the local coordination system (b) and has particular dimensions (c).

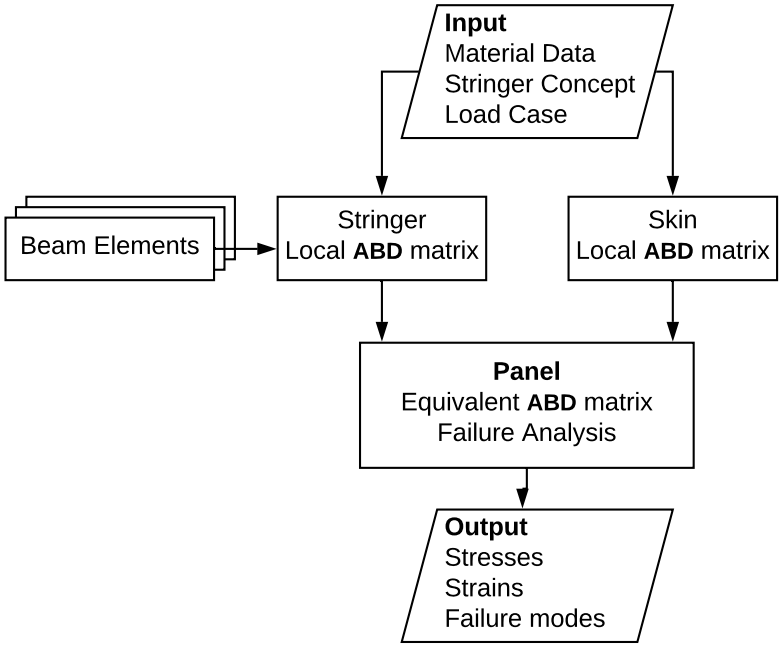

Figure 15 Flowchart of modeling the equivalent plate and access to beam class

stringer is modeled of single instances, new stringers can be defined by simply adjusting the coordinates. Once the applicability of an element is verified, the validation of further concepts can particularly focus on the composition of new concepts and their boundary conditions.

The second class defines the stiffness properties of the skin and is based on the laminates as single beam element. The third class finally determines the overall panel and combines the stiffness properties of stringer and skin. It defines the panel's dimensions and outputs the equivalent $\boldsymbol{ABD}$ matrix. In some special cases, as discovered during the derivation of the analytical formulation, the skin and stiffener interact in certain ways. Thus, the panel class has specific functions to determine the required values, since it has access to both the plate's and stiffener's data. Furthermore, the panel outputs the failure analysis for the panel, thus critical buckling loads and reserve factors.

Figure 15 gives a comprehensive flow-chart, to allocate the previously discussed classes inside the optimization environment. Referring to the problem statement in Section 1.2, the analytical formulation was derived in Section 3.3 and the present chapter described the implementation into the code. To verify the obtained method, Chapter 5 validates the formulation with respect to FEM.

5. Validation

Chapter 3 derived the analytical formulation for an arbitrary cross-section to satisfy the stated problem in Section 1.2. Followed by utilizing the obtained formulation and applying it to particular concepts, discussed in Chapter 4. Appendix C, D and E list the used equations for each stiffening concept. The objective of the present chapter is, to verify the analytical formulation, by comparing the deformation and determined failure modes, with respect to discrete FE models. In particular, errors due to simplification are investigated.

Therefore, Section 5.1 defines the prerequisites for the verification process. It elaborates on the exemplary evaluated panel, including dimensions, lay-up and boundary conditions. Followed by modeling the respective panel in a finite element environment in Section 5.2. This includes the discrete model of the panel, as well as the equivalent-plate model. The validation itself is separated into two parts. Section 5.3 verifies the resultant deformation, obtained by applying internal loads to the stiffened plate, respectively to the equivalent model. This is of importance, since the required local stresses for the failure analysis result from local compression. In Section 5.4 the optimization constraints, i.e., strength and buckling criteria, are discussed.

5.1. Panel Design

The verification process is performed with a $1500 \times 750\,\mathrm{mm}$ panel, which is braced by 5 stiffeners in longitudinal direction, as shown in Figure 16. The longer side, denoted as a, is furthermore separated by simulated spars, indicated by the dashed horizontal lines, into three subsections. This arrangement corresponds to a stiffener spacing of 150 mm and a distance between ribs of 500 mm, which is in compliance with design rules by Kassapoglou [26]. This choice also lies in an acceptable range of optimum weight evaluations conducted by various researchers, such as Ainsworth et al. [2], D. Swanson et al. [12] and Arunkumar et al. [3]. The spacing remains

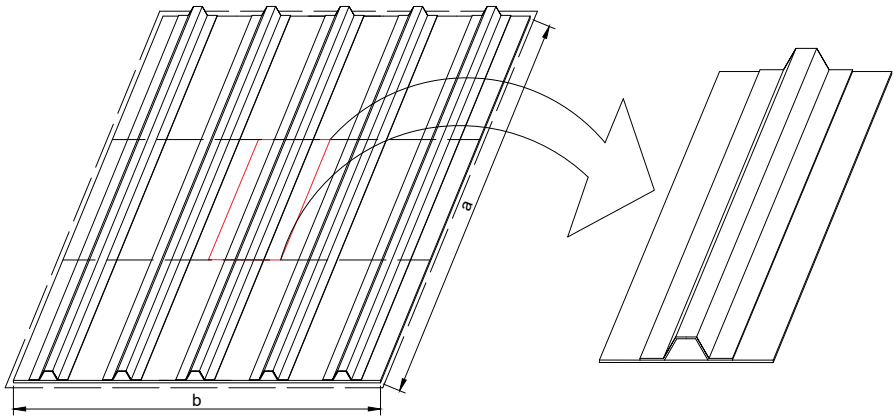

Figure 16 The panel on the left represents the discrete FE model with exemplary Ω-stringers. The validation itself is conducted with the isolated area on the right side, to reduce errors from boundary conditions.

the same for every cross-section, since the validation seeks to point out sources of error and not yet in finding the optimum panel. For errors, caused by boundary conditions to remain as low as possible, the validation is conducted with an isolated repetitive cross-section, outlined in Figure 16.

In the following, Section 5.1.1 defines the particulars of the previously discussed cross-section. Section 5.1.2 elaborates on the present laminate and material properties and Section 5.1.3 finally gives the applied load cases.

5.1.1. Stiffening Cross-Section

The conclusion of Section 4.1 was, that T-, I- and Ω-stiffener are a feasible choice for the present validation. Therefore, this section discusses the specific dimensions and Table 4 lists the particulars of each concept.

As mentioned in the stringer assessment in Section 4.1.5, the T-stiffener, in particular the foot, is taken to investigate the behavior to shear loads. The stiffeners are defined accordingly to design rules by Kassapoglou [26], who states minimum dimensions for stiffening cross-sections. Satisfying the given requirements for highly loaded plates, the stiffeners have a height of 22 mm, which remains the same throughout the validation. The thickness of each element depends on the lay-up and is discussed in Section 5.1.2.

The initial foot width of 20 mm is doubled twice, until it reaches a maximum of 80 mm, which is over 50 % of the stringer's spacing. The web is deliberately kept

Table 4 Geometrical data for stiffened concepts. Thickness is determined my laminate lay up in following section. The angle for Ω-Stringers is set between the skin and web, cf. Figure 5.

No.	Concept	Height [mm]	Foot Width [mm]	Flange Width [mm]	Web Angle [°]
1	T	22	20	-	-
2	T	22	40	-	-
3	T	22	80	-	-
4	I	22	20	19	-
5	I	22	20	10	-
6	Ω	22	19.25	17.5	90
7	Ω	22	19.37	17.74	80
8	Ω	22	19.57	18.13	60

weak to obtain global buckling.

To increase the panel's bending resistance, I-stringers with two different flange designs are taken. The goal is to investigate the flange's influence on the deformation, in particular, when applying a shear load, since it is neglected for the shear stiffness in Chapter 3 The foot width remains close to the minimum requirements, to minimize its influence.

The last concept, the Ω-stiffener, evaluates the behavior of closed profiles, since it had an extraordinary role in the previous chapters. From particular interest are two cases, the first is the ability of allowing shear flow through its elements and the resultant local shear stresses. The second is the influence on the boundary condition of the spacing span. Therefore, the web angle, is step-wise increased, which results in the ability of carrying an increasing shear flow and higher torsional stiffness, thus, rather a rigid support for the spacing span, accordingly to Sections 3.3 and 4.1.2.

5.1.2. Laminate Lay-Up

Accordingly to various books about composites materials, such as Breuer [8], certain guidelines should be followed for composite materials. However, the lay-ups used in this work, follow examples from Kassapoglou [26], which slightly differ from his own design rules and from Breuer [8].

Kassapoglou [26] suggests to use 45° layers for the web, since it carries out primarily transverse loads. Additionally, due to fabrication processes, the outer layers of the foot and if present, the flange, coincide with the outer lay-up of the web. The flange

Table 5 Material properties and particular lay-up, used for the validation.

Material Properties							
E_{11}	=	145000	MPa	E_{22}	=	8500	MPa
G_{12}	=	4500	MPa	ν	=	0.3	

Laminate lay-up			
Skin	$[45, -45, 0_2, 90]_S$		
	Foot	Web	Flange
T	$[45, -45, 0_2, 45, -45]_S$	$[45, -45, 45, -45]_S$	-
I	$[45, -45, 0_2, 45, -45]_S$	$[45, -45, 45, -45]_S$	$[45, -45, 0_2]_S$
I	$[45, -45, 0_2, 45, -45]_S$	$[45, -45, 45, -45]_S$	$[45, -45, 0_2, 90 , 0]_S$
Ω	$[45, -45, 0_2, 45, -45]_S$	$[45, -45, 0_2, 45, -45]_S$	$[45, -45, 0_2, 45, -45]_S$

for the I-stringer has additional 0° layers, which considerably increase the moment of inertia, hence, the bending and consequently the buckling resistance.

Due to modeling preconditions of the finite element model, the Ω-stringers has the same lay-up for the foot, web and crown. In the present case, it corresponds to the laminates of the open profile's foot.

5.1.3. Load Cases

Chapter 2.1 defined the resultant load paths, due to external forces. It concluded, the stiffened panel is subjected to in-plane axial and shear loads . The axial compression load is induced alongside the shorter side of the panel and equally distributed over the entire cross-section, including the stiffeners. The shear load in contrary, is only induced alongside the skin's edges and the stiffener's foot. For the validation itself, the load is separated into two sub-cases, where the first only considers axial load and the second shear loads, as listed in Table 6

Table 6 Applied load for the validation of failure modes, divided into two sub-cases.

Load Case	1	2
N_x (N/mm)	−350	-
N_y (N/mm)	-	-
N_{xy} (N/mm)	-	175

5.2. Finite Elements Model

This section defines the finite element (FE) models, required for the validation process. For the numerical analysis, MSC Patran/Nastran [11] is used. Section 5.2.1 elaborates on the discrete model, which is the reference for the conducted validation, followed by the particulars for the equivalent plate in Section 5.2.2.

5.2.1. Discrete Model

To conduct the validation, a discrete stiffened panel is modeled, accordingly to Figure 17, where for visibility, only the isolated area of interest is shown. The skin and each element of the stiffening cross-section is modeled with a *PSHELL* element, which allows to assign materials to the model. In this case, *MAT8* properties are used, which require a discrete lay-up with material properties, in this case, an orthotropic material, accordingly to Section 5.1.2.

To provide an interaction between the stiffening model and the plate, rigid body elements connect the proximity nodes, specifically *RBE2* elements, cf. Figure 17b. This enables the shared deflection of the respective nodes, i.e., same deformation as well as rotation, thus an ideal attachment.

Referring to Section 2.1 and 5.1.3, the compression force is induced over the entire cross-section, skin and stiffeners equally. The load is distributed by a multiple point constraint (MPC). The force is applied on a single node and the *MPC* issues the load to connected nodes, in the present case, along the edges of the panel. The shear load is applied at each node around the skin and the edges of the stringer's foot.

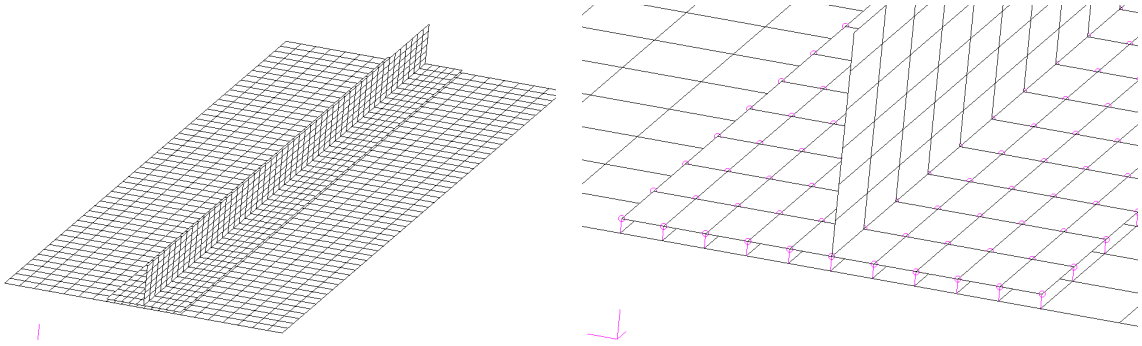

(a) Isolated area of interest **(b)** Close-up of the the skin-stringer area

Figure 17 The figure in (a) shows the isolated area of the discrete FE model and (b) focuses on the connection between stringer and foot with MPCs.

The boundary conditions are in compliance with Section 5.1 and Figure 16. The edges all around the panel, as well as the simulated ribs are simply supported, thus constrained in their z-direction.

5.2.2. Equivalent Plate

The equivalent plate model consists, analogously to the discrete model, of a *PSHELL* element with a *QUAD4* mesh. This time however, an equivalent formulation defines the assigned materials properties. Hence, the equivalent membrane, bending and coupling properties are used as input, directly. Therefore, each matrix is represented by a *MAT2* property, which contains the single stiffness terms.

The force is, analogously to the discrete panel, induced with *RBE2* elements. Due to the varying stiffness in z direction of the discrete structure, the force is induced with an eccentricity, corresponding to the stiffness weighted centroid of the panel, analogously to the derivation of second moment inertia in Section 3.3.2. Thus, the distance coincides with the neutral plane of the stiffened panel. This is of importance at this point, since the flat plate does not yield a bending moment, in contrast to the discreet model, where it is obtained due to stiffness-weighted eccentricities . Therefore, the *MPC* has an offset, which corresponds to the aforementioned neutral plane and results in an additional bending moment.

The boundary conditions are in full conformity with the discrete panel. The edges all around the panel, as well as the simulated ribs, are simply supported, thus constrained in their z-direction.

5.3. Validation of the Equivalent-Plate Model

Accordingly to the motivation in Section 1.1 and the problem statement in Section 1.2, the equivalent stiffness formulation is determined to describe the properties of the shell element, defined in Section 5.2.2. The objective of this section is, to show the validity of the equivalent-plate model. Therefore, the two previously defined load cases are subjected to the discrete as well as equivalent-shell model and the results are compared.

The first evaluation specifically focuses on in-plane strains, due to induced compression loads. Since the elements of the discrete panel have different stiffness properties, a varying longitudinal deflection is present. This in not in compliance with the state-

Table 7 Strain resultants of the discrete and equivalent FE model for open profiles.

		T_1	T_2	T_3	I_4	I_5
LC1	FEM (ε_x)	−0.003 35	−0.002 99	−0.002 48	−0.003 04	−0.003 08
	Present (ε_x)	−0.003 34	0.003 00	−0.002 49	−0.003 04	−0.003 09
	Dev.(%)	0.15	-0.33	-0.65	0.1	-0.1
	FEM (ε_y)	0.001 10	0.001 02	0.000 90	0.000 98	0.000 99
	Present (ε_y)	0.001 06	0.000 94	0.000 77	0.000 98	0.000 96
	Dev. (%)	3.31	7.40	15.38	0.61	0.10
LC2	FEM (γ_{xy})	0.007 37	0.007 04	0.005 30	0.007 37	0.007 37
	Present (γ_{xy})	0.007 36	0.006 67	0.005 29	0.007 36	0.007 36
	Dev. (%)	0.11	5.21	0.23	0.12	0.11

ment in Section 3.3, where skin and equivalent-stiffener layer share the same strains. However, as a consequence, the mean value of the deformed cross-section is taken as reference for the evaluation. The equivalent-plate model is based on the analytical formulation and defined by a shell element, with only representative thickness, thus, an even deflection is obtained.

Both discrete and shell model show highly matching results for the longitudinal strains and the deviation stays under 1 %, cf. Table 7 and 8 for open and closed profiles, respectively. However, when the foot width is gradually increased for the T-stiffened panel, the deviation slowly rises. Omitting the $(B_{33})_{\text{foot}}$ stiffness deviations below the reference are obtained. This concludes, that the foot stiffness influences the deformation, however, the magnitude for the present case is too high. For the $I_{1,2}$-stiffened panel, with a small foot, the deviation stays low.

Surprisingly, the strains in y-direction of the discrete model are higher than of the equivalent representative, since the analytical formulation neglects certain stiffness terms. However, the FE model shows varying strains along the transverse axis, since each element of the panel has its particular stiffness properties. The equivalent-shell model on the contrary, smears the stiffness over the entire shell, thus the overall stiffness leads to lower strains.

The shear shear strains of the evaluated plates, however, give less accurate results, which significantly exceed 1 %. The obtained strains are even higher than he unstiffened plate, which has shear strains of $\gamma_{xy} = 0.008\,05$. However, Table 7 and 8 list the improved values, which are obtained after some investigations and discussed now. Since $(A_{33})_{\text{panel}}$ increases due to the foot's influence, the higher shear strains are unexpected, therefore, the same iteration is conducted without $(B_{33})_{\text{stringer}}$, which significantly improves the results. When omitting the coupling, excellent results are

Table 8 Strain resultants of the discrete and equivalent FE model for closed profiles.

		$\Omega_{7,90°}$	$\Omega_{8,80°}$	$\Omega_{9,60°}$
LC1	FEM (ε_x)	−0.002 36	−0.002 34	−0.002 28
	Present (ε_x)	−0.002 36	−0.002 35	−0.002 29
	Dev. (%)	0.34	-0.38	-0.44
	FEM (ε_y)	0.000 76	0.000 76	0.000 74
	Present (ε_y)	0.000 76	0.000 76	0.000 74
	Dev. (%)	0.52	0.40	0.41
LC2	FEM (γ_{xy})	0.006 43	0.006 24	0.005 68
	Present (γ_{xy})	0.006 61	0.006 48	0.006 11
	Dev. (%)	-2.70	-3.81	-7.57

obtained, which yield deviations around 0.1 % for open structures. Referring to the reference results, the strains are slightly lower now. That shows, that the coupling terms, hence the foot, influence the shear deformation, however, not with its full stiffness as it is in the present method.

A similar behavior is obtained for the shear strains of closed profiles, but in comparison to the open profiles, the foot influences the errors slightly, since the torsional-bending resistance of the cell is the dominant factor. Neglecting the $(B_{33})_{\text{stringer}}$ term, leads to lower strains, while accounting it to slightly higher values. However, even though the actual shear strains could not be predicted as accurate as for the open profiles, the resulting shear stresses, further discussed in Section 5.4.1, show precise results.

However, for the present problem statement and scope of this thesis, only some aspects of the previously conducted validation are required. To verify the failure criteria in Section 5.4, only certain strains are of importance, primarily longitudinal and shear strains, since they are required to conduct the strength analysis in Section 5.4.1. For the buckling analysis in Section 5.4.2, the strains are not directly needed, since the critical load is determined separately, refer to Section 4.1.3. Since the required strains show sufficient results, when neglecting $(D_{33})_{\text{foot}}$ and $(B_{33})_{\text{foot}}$, the validation of constraints, used in optimization, can be conducted.

5.4. Validation of Optimization Constraint

The previous analysis showed, that deflection and strains can be properly determined with an equivalent-plate analysis. The next step is to analyze the stiffened

structure in terms of failure criteria, i.e., the required optimization constraints for Chapter 6. Therefore, the second validation is separated into two sub-parts. First, Section 5.4.1 evaluates the strength criteria for each element, by taking the overall strains and applying failure theories, discussed later. Section 5.4.2 discusses the buckling constraints, derived in Section 4.1.3 and validates the present analytical methods.

5.4.1. Strength Analysis

This section discusses the evaluation of the strength criteria, as it is one of the optimization constraints in Chapter 6. Kassapoglou [26] proposes various strength criteria, which are commonly accepted for composite materials, for example maximum stress/strain, Tsai-Wu or Tsai-Hahn. However, they all analyze each layer separately to determine the local reserve factor. As stated in Section 1.2, the present optimization environment uses a gradient-based method, which requires a continuous objective function. Therefore, IJsselmuiden et al. [24] proposed a method for lamination parameter, cf. 3.2.2, based on Tsai-Wu failure criterion. To determine the minimum allowed stress, two polynomials in terms of the reserve factor must be solved:

$$f_1(RF) = a_{12}RF^2 + a_{11}RF + a_{10}, \tag{50a}$$

$$f_2(RF) = a_{24}RF^4 + a_{23}RF^3 + a_{22}RF^2 + a_{21}RF + a_{20}, \tag{50b}$$

where the coefficients a_{ij} are dependant on the material invariants, which were introduced in Section 3.2.2 and further discussed in the paper by IJsselmuiden et al. [24]. Dähne and Hühne [13] utilize this approach in their paper and state, that Equation (50) yields up to six roots with different magnitude, where the smallest one is of importance, since it gives the lowest critical load. The used reserved factor in this thesis is defined as follows:

$$RF = \frac{\sigma_{\text{allowed}}}{\sigma_{\text{applied}}}, \tag{51}$$

where σ_{applied} is the actual stress of the evaluated element and σ_{allowed} defined by material properties, hence if $RF \geq 1$, the laminate does not fail. For the discrete model, MSC Patran/Nastran uses the maximum tension approach, which evaluates the local stresses of each ply and outputs a respective failure index (FI), which can be re-expressed with:

$$RF = \frac{1}{FI}, \tag{52}$$

Table 9 Critical buckling loads and predicted buckling modes for axial compression and shear. Values are determined with formulation defined in Appendix C to E.

		T_1	T_2	T_3	I_4	I_5	Ω_6	Ω_7	Ω_8
FEM	RF_σ	1.43	1.59	1.92	1.56	1.54	2.02	2.03	2.07
Present	RF_σ	1.43	1.59	1.91	1.57	1.55	2.02	2.03	2.08
FEM	RF_τ	1.18	1.31	1.18	1.18	1.18	1.32	1.18	1.18
Present	RF_τ	0.67	0.62	0.78	0.67	0.67	0.63	0.64	0.68

which yields conform reserve factors in regards to IJsselmuiden et al. [24].

To conduct the actual analysis, the panel is divided into its single elements, accordingly to Section 4.1.3. The in-plane stresses are then determined by the taking the local ***ABD*** matrix, substituting the strains with the respective longitudinal magnitude, taken from the equivalent-plate and finally solved for local in-plane and moment stresses.

While most elements show highly accurate results, the web of the T-stiffener deviates with increasing foot width. This behavior is due to the varying stiffness properties, previously discussed in Section 5.3. The web is higher compressed than the remaining structure and thus yields higher stresses. The strains obtained by the equivalent-plate are slightly lower, hence lower stresses. Another area of interest is the interaction of foot and skin. The discrete model analyses these two elements separately and gives different values in comparison to the present theory. This behavior is explained by accounting the transverse stresses of the skin and stringer. While it is nearly zero for the open span of skin, since the panel can deform freely in every horizontal direction, the skin under the foot, as well as the foot itself try to deform with a different magnitude, since different directional properties. If the same material is used for the skin and the foot, the transverse deformation coincides, hence no transverse stresses. However, superimposing the mean stresses of the foot and skin, yields matching results with the analytical formulation.

Table 9 shows the obtained reserve factors for the compression and shear load case. While RF_σ shows highly matching results, the analytical formulation shows failure for the shear case, in contrary to the discrete panel. This is based on the present failure method by IJsselmuiden et al. [24], which evaluates every possible angle, even if its not in the present laminate, hence a conservative approach.

5.4.2. Buckling Criteria

This section evaluates the results for the buckling criteria, cf. Section 4.1.3, since it is one of the optimization constraints. While the analytical evaluation determines the critical buckling load of each element separately, it is hardly possible with the discrete finite element model. The numerical solution calculates the eigenvalues of the panel, which represent the minimum buckling load. That means, if the panel has a high overall stiffness, the smallest eigenvalues show a critical failure load for local buckling. It is possible to solve for a great amount of eigenvalues and find a global buckling mode, but it is rather guessing and not efficient. However, for the optimization, the lowest critical buckling load, either global or local, is sufficient, since it would lead to failure of the panel. Consequently, the following validation focuses on predicting the lowest critical buckling load.

Compression Buckling

The first load case, cf. Section 5.1.3, is a uni-axial compression load. Table 10 lists the obtained critical buckling loads for open profiles, while Table 11 contains the data for closed profiles. As anticipated, the T-stiffened panel's failure mode is global buckling, and accurately predicted by the analytical formulation. Since the HSB [1] provided equation for the critical buckling load is a conservative approach, a deviation of under 5 % is acceptable and within a range of previously mentioned papers, such as by Bisagni and Vesconi [6]. For $T_{2,3}$, however, the analytical load yields higher critical buckling loads with increasing foot width. Referring to Section 5.3, the influence of the foot has occurred errors once before. As the deviation increases in the present case analogously, it could be the potential problem, again. Conducting the analysis without the $(D_{22,33})_{\text{foot}}$ and $(B_{22,33})_{\text{foot}}$ terms, the obtained buckling load stays significantly below the reference. This means, that the foot definitely increases the global buckling mode, however, the ratio of foot width to spacing, as it is used here, determines too high stiffness terms.

Table 10 Critical buckling loads and predicted buckling modes for axial compression. Values are determined with formulation defined in Appendix C to E

	T_1	T_2	T_3	I_4	I_5
FEM (N/mm^2)	−17.34	−18.49	−20.76	−41.52	−40.60
Present (N/mm^2)	−17.08	−19.35	−21.77	−40.73	−40.73
Dev. (%)	4.42	−1.86	−2.22	1.91	−0.30
Mode	Global	Global	Global	Local	Local

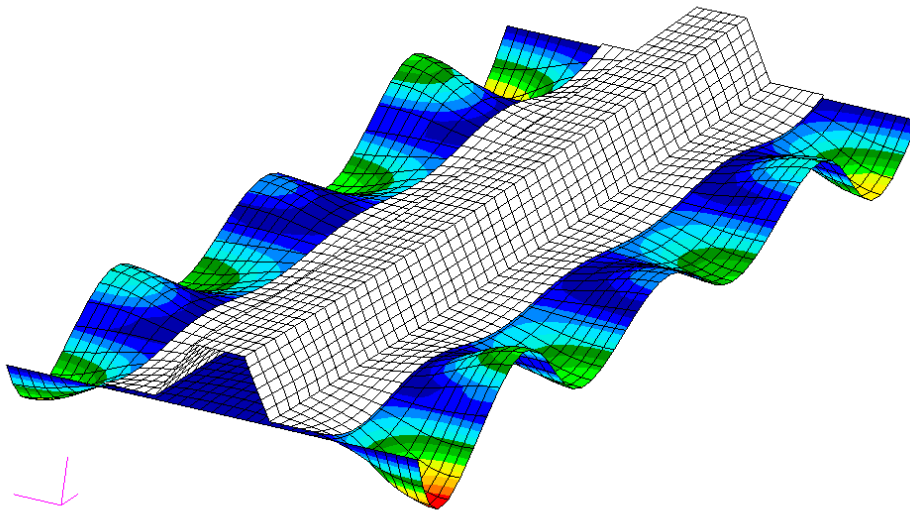

Figure 18 FEM compression buckling deformation of Ω-stiffened skin. The red color indicates the maximum, while blue represents the minimum. The foot is not colored for clarity, but takes the same color as the adjacent areas, hence, blue.

For the I- and Ω-stiffened panel, local buckling of the spacing span occurs, i.e., the skin as well as the foot buckle and is shown exemplary for the latter in Figure 18. As seen in Table 10, the critical buckling load for I-stiffened panels could accurately be predicted, with an accuracy of under 2 %. This shows, that a simple support, as discussed in Section 4.1.3, is a valid assumption for open profiles.

For the Ω-braced panel on the contrary, mixed results are obtained. While for high angles, cf. $\Omega_{6,90°}$, the load shows acceptable results, though conservative, the deviation significantly increases for $\Omega_{8,60°}$. In Section 5.4.2, the exceptional behavior of closed structures and their influence on the inner span was already discussed. To further investigate the behavior, more analytical calculations are conducted. Assuming clamped conditions, as proposed by Kassapoglou [26], the analytical solutions yields too high buckling loads for small angles, but accurate critical laods for small angles. Hence, clamped boundary conditions can be an appropriate assumption, depending on the present cross-section. However, since Kassapoglou [26] does not specify when this is the case, it is not an eligible method for the present theory. To predict

Table 11 Critical buckling loads and predicted buckling modes for axial compression. Values are determined with formulation defined in Appendix C to E

	$\Omega_{6,90°}$	$\Omega_{7,80°}$	$\Omega_{8,60°}$
FEM (N/mm^2)	−98.31	−114.74	−222.03
Present (simple)(N/mm^2)	−72.49	−83.60	−118.99
Present (clamped)(N/mm^2)	−136.47	−158.31	−228.59
Mittelstedt and Beerhorst [35](N/mm^2)	−107.85	−120.11	−196.26

the boundary conditions more specifically, Mittelstedt and Beerhorst [35] derived a formulation for elastically restrained orthotropic composite plate, i.e. adjustable boundary conditions, depending on the local stiffness of the Ω-stringer. It was discussed in Section 4.1.3 and implemented into the present method, accordingly to Appendix B. The results are listed in Table 11 and yield much better results for the buckling of the spacing span.

The validation of the critical axial compression load showed, that failure modes, either global or local can accurately be predicted. It further showed, unveiled, that simple support are eligible for open profiles, while closed profiles must account elastic constraints to yield accurate results for all web angles.

Shear Buckling

As discussed in Section 4.1.3, the shear buckling is a less predictable load case, particularly asymmetrical laminates are not specifically accounted in the given equation for critical shear buckling loads. However, taking the provided Equation from the HSB [1] in combination with the corrected $\tilde{\boldsymbol{D}}$ matrix from Equation (41), the global shear buckling load for T-stiffened panels is accurately be predicted, as listed in Table 12.

Analogously to compression failure Figure 19 shows the failure of of the spacing span, thus, skin and foot simultaneously. However, the involved area of the foot is much smaller in comparison to compression, where nearly the entire foot deforms equally. This also reflects in the obtained critical buckling loads by the analytical formulation. Therefore, various calculations are conducted to investigate the most eligible failure prediction.

Since the foot lead to errors before, the validation is conducted again, while subsequently either $(D_{22,33})_{\text{foot}}$, $(B_{22,33})_{\text{foot}}$ or both are omitted. Without $(D_{22,33})_{\text{foot}}$ and $(B_{22,33})_{\text{foot}}$ the critical buckling load is too low and omitting $(D_{33})_{\text{foot}}$ and $(B_{33})_{\text{foot}}$ yields to too high values. When only $(D_{22})_{\text{foot}}$ and $(B_{22})_{\text{foot}}$ is set to zero,

Table 12 Critical shear buckling load for panel braced with open-profiles stringers.

	T_1	T_2	T_3	I_4	I_5
FEM (N/mm^2)	18.77	22.65	34.68	29.94	29.26
Present(Spacing span) (N/mm^2)	20.48	22.89	25.64	52.98	52.98
Present ($(D_{22}, B_{22})_{\text{foot}} = 0$) ($N/mm^2$)				31.72	31.72
Present (Open span) (N/mm^2)				30.31	30.31

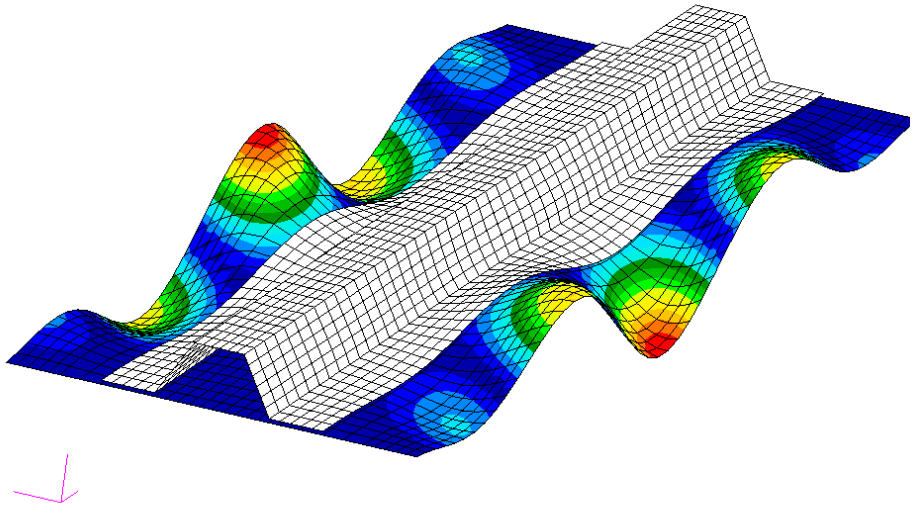

Figure 19 FEM shear buckling deformation of Ω-stiffened skin. The red color indicates the maximum, while blue represents the minimum. The foot is not colored for clarity, but takes the same color as the adjacent areas, hence, primarily blue.

however, the present method yields deviations with the magnitude comparable to the compression buckling load and conservative results for Ω, again.

However, another interesting outcome was obtained for the buckling of the open span, i.e., the foot is not accounted. Even though the foot buckles with the skin, cf. Figure 19, the buckling load can quite precisely be predicted for the aforementioned open span, for every present case. However, in contrary to the compression buckling case, where a simple support at the transition zone from open span to foot yield too conservative buckling loads, thus a clamped support was assigned, the present method predicts the magnitude accurately, as seen in Tables 12 and 13.

The evaluation of the critical shear load concluded some interesting facts. First of all, it is a rather less predictable case, where the foot influence varies between open and closed profiles. However, the difficulty with shear deformation is not new and mentioned in various papers, such as by Dähne and Hühne [13]. However, for the present cases, the buckling load could predicted properly after some further investigations. Therefore, for the following application the boundary conditions for the open span are assumed as simply supported, since it showed accurate results.

Table 13 Critical shear buckling load for panel braced with closed-profiles stringers.

	$\Omega_{7,90°}$	$\Omega_{8,80°}$	$\Omega_{9,60°}$
FEM (N/mm^2)	56.51	64.72	109.84
Present (Spacing span) (N/mm^2)	96.94	111.56	158.38
Present (Open span) (N/mm^2)	55.85	65.82	101.41

5.5. Discussion

In Section 5.4, numerical and analytical calculations were conducted to verify the formulation, derived in Chapter 3. Therefore, pre-defined braced panels were evaluated in terms of failure modes, that included strength criteria and critical buckling loads. The initial validation was conducted with the obtained stiffness matrices determined by equations listed in Appendix C to E and defined boundary conditions accordingly to literature and listed in Table 3.

Particularly the validation of the reserve factors for the compression load case achieved highly accurate results. Furthermore, the critical buckling load was predicted with sufficient errors. For the local bucking of Ω-braced plates, conservative results were obtained. However, altering the boundary conditions in correspondence to Kassapoglou [26] and Mittelstedt and Beerhorst [35], better results could be predicted, depending on the actual cross-sectional dimensions.

The compression as well as the buckling evaluation additionally gave interesting results. The foot, even though omitted by Nemeth [37] and Kassapoglou [26], definitely increases the buckling stiffness of the overall panel as well as of the spacing span, where it is "smeared" into skin. The magnitude however, differs from the present method. Particularly the shear compression showed reliance on the foot's influence, specifically the $(D_{22})_{\text{foot}}$ and $(B_{22})_{\text{foot}}$ deviates the terms negatively. Without however, accurate results were obtained for I-stiffened panels and a conservative load for Ω-braced panels. For shear buckling another interesting behavior was discovered, by assuming simple boundary conditions for the open span, precise critical buckling loads were obtained, even though, referring to the FE analysis and illustrated in Figure 19 the buckling of the spacing span is the area, which fails. The strength analysis of the shear load case yielded conservative results, which is based on the used method for lamination parameter, where all angles are evaluated.

Accordingly to the problem statement in Section 1.2, an equivalent-plate stiffness was derived in Chapter 3 and the present chapter validated it with respect to a discrete finite element model. As the results show highly sufficient results, the analytical formulation of the equivalent shell model can be used for further purposes. To show its applicability inside the optimization environment, Chapter 6 conducts optimization runs in a defined scenario.

6. Application

The objective of the discussed analytical formulation in Chapter 3, as well as the verification of failure modes in Chapter 5 was conducted to seek an eligible formulation for stiffness properties of a braced panel. In this chapter, the present method is utilized to conduct an optimization of a stiffened panel.

Therefore, Section 6.1 elaborates on the mathematical formulation of an optimization method and applies the derived equations to the present scenario. Section 6.2 describes the work-flow of the optimization environment and in Section 6.3 the results are finally discussed.

6.1. Optimization Problem

The objective of optimization problems is to alter an initial design with respect to certain design variables and find the optimum, thus most efficient structure, while satisfying defined boundary conditions. To achieve this goal, various methods were proposed, such as by Bisagni and Vesconi [6], Herencia et al. [23] and IJsselmuiden et al. [24]. The present optimization environment at DLR uses a gradient-based method, developed by Dähne and Hühne [14] and extended by Werthen and Dähne [49].

Therefore, Section 6.1.1 discusses the aforementioned method and states the mathematical formulation. Section 6.1.2 applies the formulation to the present problem and defines design variables as well as constraints.

6.1.1. Mathematical Formulation

The goal of optimization problems is to minimize an objective function $f(\boldsymbol{x})$, in terms of pre-defined design variables. The present problem is a multi-variable op-

timization, i.e., an arbitrary amount of variables alter $f(\boldsymbol{x})$, therefore, the vector $\boldsymbol{x}$ defines a set of design variables. To satisfy certain boundary conditions, the objective functions can be constraint, i.e., $g_i(\boldsymbol{x})$ must be fulfilled. Consequently, the problem is described as:

$$\min f(\boldsymbol{x}), \tag{53}$$

subjected to

$$g_i(\boldsymbol{x}) \leq 0, \tag{54}$$

$$x_j^{\mathrm{l}} \leq x_j \leq x_j^{\mathrm{u}}, \tag{55}$$

where

$$\boldsymbol{x} = \{x_1, x_2, ..., x_n\}^{\mathrm{T}} \tag{56}$$

and $x_j^{\mathrm{l}}, x_j^{\mathrm{u}}$ are lower and upper bounds of the design variables, respectively. To conduct the gradient-based optimization, the finite differences of the objective function

$$f'(\boldsymbol{x}) = \frac{f(\boldsymbol{x}+h) - f(\boldsymbol{x})}{h}, \tag{57}$$

as well as of the constraints

$$g'(\boldsymbol{x}) = \frac{g(\boldsymbol{x}+h) - g(\boldsymbol{x})}{h} \tag{58}$$

are determined. The variable h is the step-length for the next iteration and here based on experience. The iteration stops when $f(\boldsymbol{x})$ converges and all $g(\boldsymbol{x}) \leq 0$.

6.1.2. Applied Optimization Formulation

This section applies the previously discussed mathematical formulation to the present problem. Therefore, the objective function $f(\boldsymbol{x})$, the design variables in $\boldsymbol{x}$, as well as the constraints $g(\boldsymbol{x})$ are discussed.

Objective Function

The objective of this scenario is to minimize the overall structural weight of a stiffened panel, while sustaining external and internal loads. Hence, the objective function reads

$$M(\boldsymbol{x}) = a\left(\rho_{\mathrm{plate}} A_{\mathrm{plate}}(\boldsymbol{x}) + m\sum_{n=1}^{i} \rho_j A_j(\boldsymbol{x})\right), \tag{59}$$

where a is the long side of the skin, ρ the density of either the skin or stringer, m the number of stringers and j represents each element of the stiffening cross-section. A is the effective area of the skin and dependant on the design variables, as discussed now.

Design Variables

The objective function in Equation (59) depends on a set of particular design variables, which are stored in the vector $\boldsymbol{x}$. For brevity three cases are considered:

$$\boldsymbol{x} = \{\boldsymbol{x}_i, \boldsymbol{x}_j, \boldsymbol{x}_k\}, \tag{60}$$

where the vectors with indices i, j and k contain the lamination parameter, stiffener geometry and panel dimensions, respectively. The lamination parameter are discussed in Section 3.2.2, the stiffener's variables determine the dimensions, such as height, web thickness or food width. The last set finally determines the overall panel, such as stiffener spacing.

Optimization Constraints

The mathematical formulation allows to constrain the objective function, in the present case, the optimization must satisfy the failure criteria. As stated in Section 6.1.1, the constrained function must yield a value lower than 0. Therefore, analogously to the strength criteria in Section 5.4.1, the reserve factor RF for buckling is determined with:

$$g_{\text{buckling}}(x) = \frac{1}{RF_{\text{buckling mode}}} - 1 = \frac{N_{\text{applied load}}}{N_{\text{critical load}}} - 1 \leq 0, \tag{61}$$

where the subscript corresponds to each buckling modes Additionally reserve factor for the strength analysis, accordingly to Section 5.4.1, yields:

$$g_{\text{strength}}(x) = RF_{\text{strength criteria}} - 1 \leq 0. \tag{62}$$

Since $g(\boldsymbol{x})$ must be lower zero, 1 is subtracted from the RF in Equations (61) and (62) The lamination parameter are constraint accordingly to Herencia et al. [23].

6.2. Optimization Environment

Accordingly to Figure 20, this section discusses the iterative process of minimizing the objective function. To start the iteration, initial design parameters $\boldsymbol{x}_0$ as well as the objective function and constraint functions are defined. With these parameters, the equivalent-plate is modeled and with the analytical formulation, as discussed in Chapter 3, the constraints are determined. As optimizer, the open optimization framework NLopt[1] with MMA algorithm, developed by Svanberg [46] is used, inside and Python[2] environment.

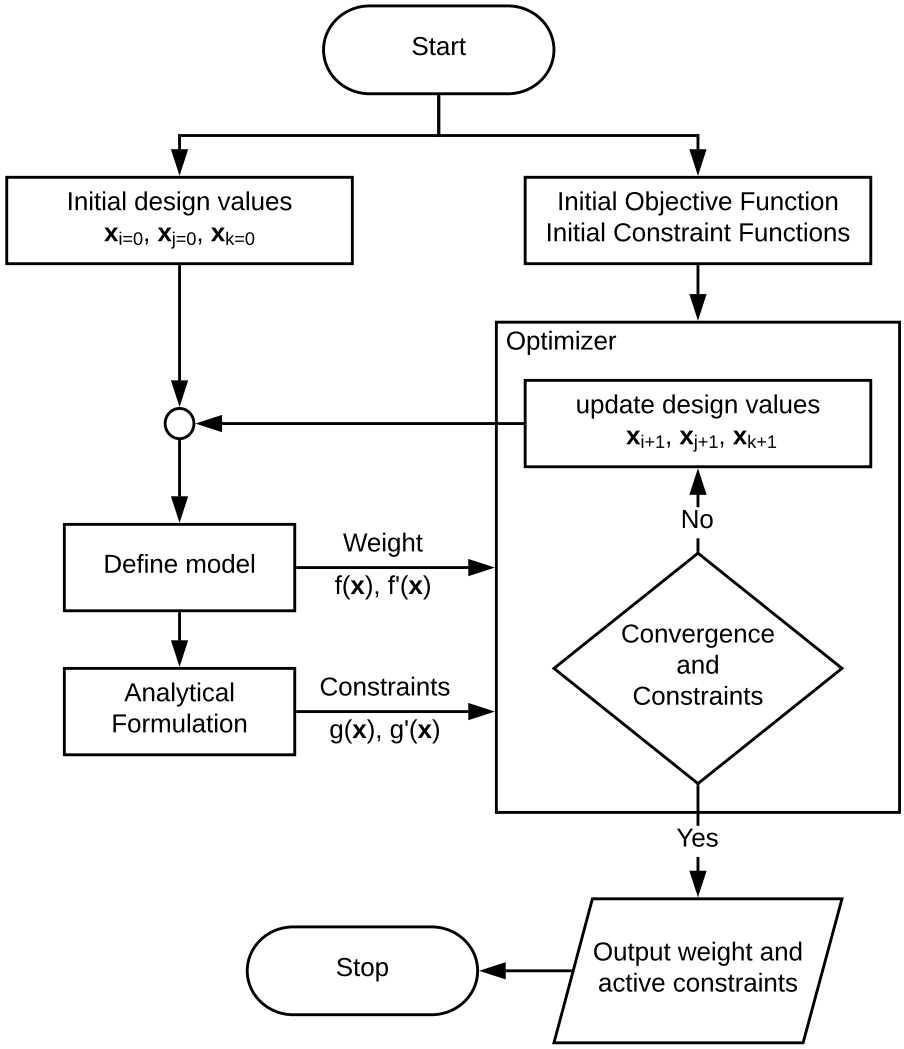

Figure 20 Optimization flowchart, where the left side represents the analytical formulation and the right side the optimization environment.

[1] `https://nlopt.readthedocs.io`
[2] `https://www.python.org`

The optimizer evaluates the constraints and the convergence criteria of the objective function. If it fails, it updates subsequently each variable and evaluates the aforementioned criteria again. The iteration repeats until all constraints are satisfied and the objective function converges, hence, outputs the minimum weight

6.3. Discussion

In Section 6.1.1, mathematical formulation was discussed then to be applied to the problem in Section 6.2. To verify the plausibility of the used optimization method, this section discusses the results of a stiffened plate in comparison to a scenario analyzed by Herencia et al. [23]. Therefore, a panel with dimensions of $762 \times 203.2\,\mathrm{mm}$, braced by one T-stringer and subjected to both axial and shear loads, with $-3502.54\,\mathrm{N/mm^2}$ and $-875.63\,\mathrm{N/mm^2}$, respectively, is defined. The failure criteria in the mentioned paper, however, varies slightly from the derived method, which potentially leads to small deviations of the objective function. Since Herencia et al. [23] does not depict any material strength properties, the maximum strain criterion is implemented analogously, with a maximum of 3600 and 7200 microstrains for compression and shear, respectively. Optimizing the presented objective function in Equation (59), gives a weight of 2.42 kg, which in vicinity of the obtained weight by Herencia et al. [23] with 2.45 kg. Hence, the optimizer with the present analytical formulation can used for further applications.

Since the plausibility was confirmed, the next scenario aims for comparing the newly implemented methods, in particular the difference between blade-, T- and

Table 14 Material properties for the optimization, where (a) is used for the plausibility check and (b) for the comparison of different concepts [23, 13].

(a) AS4/3502

E_{11} $(\mathrm{N/mm^2})$	127 553
E_{22} $(\mathrm{N/mm^2})$	5998
G_{12} $(\mathrm{N/mm^2})$	11 307
ν_{12}	0.3
ρ $(\mathrm{kg/mm^3})$	1.578×10^{-6}
t (mm)	0.132
$\varepsilon_{\mathrm{x,max}}$	3500×10^{-6}
$\gamma_{\mathrm{xy,max}}$	7200×10^{-6}

(b) T800/M21

E_{11} $(\mathrm{N/mm^2})$	134 600
E_{22} $(\mathrm{N/mm^2})$	7700
G_{12} $(\mathrm{N/mm^2})$	4200
ν_{12}	0.369
ρ $(\mathrm{kg/mm^3})$	1.59×10^{-6}
t (mm)	0.132
X_{T} $(\mathrm{N/mm^2})$	2290.5
X_{C} $(\mathrm{N/mm^2})$	1051
Y_{C} $(\mathrm{N/mm^2})$	41.43
Y_{C} $(\mathrm{N/mm^2})$	210
S $(\mathrm{N/mm^2})$	69.4

Ω-stringers. Therefore, a $1000 \times 2000\,\mathrm{mm}$ panel, braced by stringers and subjected to compression and shear loads with $-3500\,\mathrm{N/mm^2}$ and $-880\,\mathrm{N/mm^2}$, respectively, is analyzed. The load is furthermore separated into three load cases, compression only, shear only and combined. The used material is T800/M21 and the particulars are listed in Table 14b. The objective and constraint functions were discussed in Section 6.1.2. The design variables, as well as upper and lower bounds, are listed in Table 15. As stated in Section 3.2.2, it is possible to predict the required amount of ply angles for the used laminate with the lamination parameter. It is described in detail by Werthen and Dähne [49] and corresponds to Figure 7 in Section 3.2.2, where the feasible domain is illustrated.

For load case 1, thus, compression only, the skin has a mixed lay-up, in which each angle is present. On the contrary, the web has a rather dominant stacking of 0° layers, since it primarily influences the panel in longitudinal direction and is seen by the positive values of $V^{\mathrm{A}}_{1,2,w}$. The web of the blade-stiffened panel, takes a significant part of the overall weight, as it is the critical buckling constraint and consequently

Table 15 Lower and upper bounds, as well as optimization results for blade-stiffened panels.

Design Variables	Constraints lb	ub	Blade LC1	LC2	LC3
$V^{\mathrm{A}}_{1,\mathrm{s}}$	-0.99	0.99	0.07	0.0	−0.02
$V^{\mathrm{A}}_{2,\mathrm{s}}$	-0.99	0.99	0.01	−0.99	−0.35
$V^{\mathrm{D}}_{1,\mathrm{s}}$	-0.99	0.99	0.06	−0.01	−0.13
$V^{\mathrm{D}}_{2,\mathrm{s}}$	-0.99	0.99	−0.05	−0.97	0.09
$V^{\mathrm{A}}_{1,\mathrm{w}}$	-0.99	0.99	0.25	0.99	0.81
$V^{\mathrm{A}}_{2,\mathrm{w}}$	-0.99	0.99	0.2	0.99	0.62
$V^{\mathrm{D}}_{1,\mathrm{w}}$	-0.99	0.99	0.12	0.97	0.53
$V^{\mathrm{D}}_{2,\mathrm{w}}$	-0.99	0.99	−0.13	0.97	0.06
$V^{\mathrm{A}}_{1,\mathrm{f}}$	-0.99	0.99	-	-	-
$V^{\mathrm{A}}_{2,\mathrm{f}}$	-0.99	0.99	-	-	-
$V^{\mathrm{D}}_{1,\mathrm{f}}$	-0.99	0.99	-	-	-
$V^{\mathrm{D}}_{2,\mathrm{f}}$	-0.99	0.99	-	-	-
t_{skin} (mm)	0.5	300	6.29	5.84	9.56
t_{web} (mm)	0.5	300	10.13	lb	12.98
t_{foot} (mm)	0.5	100	-	-	-
t_{crown} (mm)	20	100 -	-	-	
φ_{web} (°)	60	90	-	-	-
w_{foot} (mm)	20	100	-	-	-
h_{stringer}(mm)	20	300	78.54	140.26	79.24
d_{s} (mm)	150	500	151.61	254.94	290.8
m_{panel} (kg)			36.68	19.43	41.76

requires a thick laminate. For the T-stiffened panel, thinner laminates can be used, however, the weight is slightly above the blade stringer. The Ω stiffened panel yields the lightest structure, this is reached by a thin laminates for every structure and the stringer is less affected by critical buckling, since each element is simply supported all around.

For load case 2, shear load only, the lamination parameters for the skin show a thick plain $\pm 45°$ laminate, cf. $V^{\mathrm{A}}_{1,\mathrm{s}} = 0$ and $V^{\mathrm{A}}_{2,\mathrm{s}} = -0.99$ in Table 15 and 16. This is a plausible result, since the skin carries the entire shear load. The web on the other hand reaches the lower bound for its thickness and has a dominant $0°$ lay-up to increase the panel's global critical buckling. The web of the T-stiffened panel shows a similar result, but the foot additionally develops shear stresses, thus, supports the skin. However, the skin and foot take the exact same values, which is based on the presented implementation, where skin and foot are evaluated separately. For the Ω-stiffened panel, a nearly fully $45°$ ply laminate is obtained for the entire structure, since the web allows shear flow, which is in compliance with the discrete FE model. Additionally, the web angle reaches the lower bound of $60°$. This correlates to

Table 16 Optimization results for T- and Ω-stiffened panels.

Design Variables	T LC1	T LC2	T LC3	Ω LC1	Ω LC2	Ω LC3
$V^{\mathrm{A}}_{1,\mathrm{s}}$	−0.3	0.0	0.09	−0.54	0.0	0.13
$V^{\mathrm{A}}_{2,\mathrm{s}}$	0.08	−0.99	−0.26	0.18	−0.99	−0.05
$V^{\mathrm{D}}_{1,\mathrm{s}}$	−0.02	−0.01	0.09	−0.18	−0.01	0.17
$V^{\mathrm{D}}_{2,\mathrm{s}}$	−0.22	−0.97	0.1	−0.4	−0.97	0.71
$V^{\mathrm{A}}_{1,\mathrm{w}}$	0.58	0.99	0.25	0.52	0	0.42
$V^{\mathrm{A}}_{2,\mathrm{w}}$	0.64	0.99	0.19	0.75	−0.99	0.3
$V^{\mathrm{D}}_{1,\mathrm{w}}$	0.13	0.97	9	0.01	0	−0.08
$V^{\mathrm{D}}_{2,\mathrm{w}}$	0.1	0.97	0.08	−0.34	−0.97	0.06
$V^{\mathrm{A}}_{1,\mathrm{f}}$	0.07	0	0.07	-	-	-
$V^{\mathrm{A}}_{2,\mathrm{f}}$	0.24	−0.99	−0.02	-	-	-
$V^{\mathrm{D}}_{1,\mathrm{f}}$	0.03	−0.01	iv	-	-	-
$V^{\mathrm{D}}_{2,\mathrm{f}}$	0.1	−0.97	iv	-	-	-
t_{skin} (mm)	3.03	5.84	10.63	1.38	5.84	11.93
t_{web} (mm)	4.74	lb	3.03	4.06	3.99	11.61
t_{foot} (mm)	3.94	5.84	11.44	4.06	11.61	11.61
t_{crown} (mm)	-	-	-35.3	11.61	20	23.21
w_{foot} (mm)	51.73	80.65	57.77	26.31	20	20
φ_{web} (°)	-	-	-	78.41	60	86.68
h_{stringer} (mm)	72.35	102.46	82.751	22.4	20	21.92
d_{s} (mm)	lb	274.94	215.56	150.03	333.42	345.13
m_{panel} (kg)	20.84	20.47	46.74	15.16	22.25	46.91

the Bredt's formula, where the area of a closed section significantly increases the torsional stiffness due to shear stresses.

Finally, for load case three both loads are combined and, as expected, it yields the highest weight. From the lamination parameter, one can conclude, that the skin develops shear stresses due to negative $V_{2,\mathrm{s}}^{\mathrm{A}}$ values and $V_{1,\mathrm{s}}^{\mathrm{A}}$ in vicinity of zero what is in compliance with the derivation in Chapter 3. A surprising result is obtained between the T- and blade stringer, since the foot carries shear stresses and was supposed to relieve the skin. The reason is, once again, the separate evaluation of the skin and stringer, which deviates the obtained minimized weight function negatively. The Ω leads to the heaviest design and the optimizer interferes in the same way between foot and skin. However, it also shows that the spacing of the Ω-stiffened panel gives the highest values, since the critical loads for inter stiffener buckling yields higher loads, as discussed during the validation in Chapter 5.

This chapter utilized the derived formulation from Chapter 3 and optimized two of the evaluated concepts from Chapter 4 in terms of minimizing the panel's weight. Additionally, the blade stringer was analyzed, as it showed good results in works by Dähne and Hühne [13]. The optimizer correctly alters the concept's geometries in terms of occurring load paths and tailors structure to obtain a lightweight design.

7. Conclusion and Future Work

The concept of smearing a stringer into an equivalent-plate model and describing the stiffness properties with an analytical formulation is an efficient method to optimize a structure in terms of minimizing weight. It allows the substitution of complex structures, in particular discrete finite element models, with so-called shell elements to conduct preliminary studies. Stiffening structures of arbitrary shape can be described with the analytical formulation and just by altering the shell model's properties, accurate deformation and eventually stresses of each element can be determined. This further allows the utilization of optimization methods and to constrain the objective weight function to desired failure modes.

This objective was approached by superimposing the stiffness matrices of both skin and stringer, where the latter is described by the aforementioned equivalent-plate. The individual consideration of skin and stringer offers remarkable advantages, not only for the optimization, but also for the implementation into the base code. The complex structure of the stiffening concept is broken down to a single laminate with well known properties. When implementing new stiffening concepts, instances of the base element, i.e., a flat laminate, are arranged to the desired cross-section, where only the element's coordinates and boundary conditions must be adjusted.

This thesis successfully showed, that the approach is well-suited for the determination of an equivalent shell model in combination with gradient based optimization. It additionally allows simple implementation of new concepts to enhance preliminary studies for the structural wing design. To even improve the discussed approach in future work, the skin foot interaction is of importance. The validation proved, that it can significantly influence the panel's local buckling behavior, however, in a non-linear way. Furthermore, the evaluated concepts are just a small selection and variety. Specifically the obtained boundary conditions are severely dependant on the stiffening concepts. To appropriately determine the inaccuracies, based on

assumptions and simplifications for the analytical formulations, parameter studies must be conducted to improve the method even further.

This thesis showed the feasibility of the equivalent shell concept with a small selection of stiffening geometries and offered a base for simple implementation of arbitrary concepts. Further research in this area could significantly improve performance of aircraft through better structural wing design and eventually increase efficiency of preliminary studies, thus development of new design.

Bibliography

[1] *Luftfahrttechnisches Handbuch für Strukturberechnung (HSB).* IASB Industrie Ausschuss Struktur Berechnunsunterlagen, 209.

[2] J. Ainsworth, C. Collier, P. Yarrington, R. Lucking, and j. Locke. Airframe wingbox preliminary design and weight prediction. In *69th Annual Conference, Virginia Beach, Virginia*, page 41. Society of Allied Weight Engineers, Inc., 05/2010 2010.

[3] K. N. Arunkumar, N. Lohith, and B.B.Ganesha. Effect of ribs and stringer spacings on the weight of aircraft composite structures. 9:433–439, 04 2014.

[4] E. Barkanov, O. Ozolins, E. Eglitis, F. Almeida, M. Bowering, and G. Watson. Optimal design of composite lateral wing upper covers. part i: Linear buckling analysis. *Aerospace Science and Technology*, 38:1 – 8, 2014. doi: https://doi.org/10.1016/j.ast.2014.07.010.

[5] E. Barkanov, E. Eglitis, F. Almeida, M. Bowering, and G. Watson. Optimal design of composite lateral wing upper covers. part ii: Nonlinear buckling analysis. *Aerospace Science and Technology*, 51:87 – 95, 2016. doi: https://doi.org/10.1016/j.ast.2016.01.020.

[6] C. Bisagni and R. Vesconi. Fast tool for buckling analysis and optimization of stiffened panels. *Journal of Aircraft*, 46(6), 2009. doi: https://doi.org/10.2514/1.43396.

[7] Boeing. Current matket oulook. `https://www.boeing.com/commercial/market/current-market-outlook-2017/`, 2016.

[8] U. P. Breuer. *Commercial Aircraft Composite Technology.* Springer, 2016. ISBN 9783319319186.

[9] B. H. Coburn, Z. Wu, and P. M. Weaver. Buckling analysis of stiffened variable angle tow panels. *Composite Structures*, 111:259 – 270, 2014. doi: https://doi.org/10.1016/j.compstruct.2013.12.029.

[10] C. S. Collier. *Thermoelastic Formulation of Stiffened, Unsymmetric Composite Panels for Finite Element Analysis of High Speed Aircraft.* AIMASME/ASCE/AHS/ASC 35th Structures, Dynamics, & Materials Conference 1994, 1994.

[11] M. S. Corporation. Msc nastran 2016.1 - quick reference guide. 2016.

[12] G. D. Swanson, Z. Gurdal, S. , and J. H. Structural efficiency study of graphite-epoxy aircraft rib structures. 27, 02 1988.

[13] S. Dähne and C. Hühne. Efficient gradient based optimization approach of composite stiffened panels in multidisciplinary environment. In *5th Aircraft Structural Design Conference 2016*, 2016.

[14] S. Dähne and C. Hühne. Gradient based structural optimization of a stringer stiffened composite wing box with variable stringer orientation. In *WCSMO 12*, June 2017.

[15] M. Duchesne. Bombardier CSeries aircraft awarded transport Canada flight test permit. `http://www.bombardier.com/en/media/newsList/details.20130830-bombardieraerospacebombardiercseriesaircraftawardedtran.bombardiercom.html`, 2013. [Online; accessed 27-November-2017].

[16] C. Fualdes. Experience & lessons learned of a composite aircraft. `http://www.icas.org/media/pdf/ICAS%20Congress%20General%20Lectures/2016/2016%20Composite%20Aircraft%20Fualdes.pdf`, 2016. [Online; accessed 27-November-2017].

[17] G. Gardiner. Cseries composite wing. `https://www.compositesworld.com/blog/post/cseries-composite-wing`, 2013. [Online; accessed 27-November-2017].

[18] D. Gates. Boeing 787 may not fly this year. `https://www.seattletimes.com/business/boeing-aerospace/boeing-787-may-not-fly-this-year/`, 2009. [Updated July 22, 2009, Online; accessed 07-July-2018].

[19] D. Gates. Local firms' gear will build challenger to Boeing 737. `https://www.seattletimes.com/business/local-firms-gear-will-build-challenger-to-boeing-737/`, 2010. [Online; accessed 27-November-2017].

[20] A. Gillessen. Continuous high volume part production technologies. `http://cfk-valley.com/fileadmin/img/downloads/INNOVATION_DAY_`

Continuous_Production/6._Vortrag_Continuous_high_volume_part_production_technologies.pdf, 2016. [Online; accessed 27-November-2017].

[21] F. Gruttmann and W. Wagner. Shear correction factors for layered plates and shells. *Computational Mechanics*, 59(1):129–146. doi: https://doi.org/10.1007/s00466-016-1339-2.

[22] H. Hahn and S. Tsai. *Introduction to Composite Materials*. Taylor & Francis, 1980. ISBN 9780877622888.

[23] J. E. Herencia, P. M. Weaver, and M. I. Friswell. Optimization of anisotropic composite panels with t-shaped stiffeners including transverse shear effects and out-of-plane loading. *Structural and Multidisciplinary Optimization*, 37(2):165–184, 2008. doi: https://doi.org/10.1007/s00158-008-0227-6.

[24] S. T. IJsselmuiden, M. M. Abdalla, and Z. Gürdal. Implementation of strength-based failure criteria in the lamination parameter design space. *AIAA Journal*, 47(7):1826–1834, 2008. doi: https://doi.org/10.2514/1.35565.

[25] J. C. Kako, Y. C. Roth, and A. Etzkorn. A30xwb wing upper cover stringer production. http://www.cfk-convention.com/fileadmin/Convention_2013/Referenten/Vortraege/CFK_Conv2013_KAKO.pdf, 2016. [Online; accessed 27-November-2017].

[26] C. Kassapoglou. Design and analysis of composite structures with applications to aerospace structures /, 2013.

[27] A. Khani, S. IJsselmuiden, M. Abdalla, and Z. Gürdal. Design of variable stiffness panels for maximum strength using lamination parameters. *Composites Part B: Engineering*, 42(3):546 – 552, 2011. doi: https://doi.org/10.1016/j.compositesb.2010.11.005.

[28] S. N. C. S. V. Kulkarni. Shear correction factors for laminated plates. *AIAA Journal*, 17(5):498–499, 1979. doi: https://doi.org/10.2514/3.61160.

[29] Y. Leach and M. Birtel. Boeing 787 dreamliner completes first flight. http://boeing.mediaroom.com/2009-12-15-Boeing-787-Dreamliner-Completes-First-Flight, 2009. [Online; accessed 7-July-2018].

[30] D. Liu, V. Toropov, M. Zhou, D. Barton, and O. Querin. Optimization of blended composite wing panels using smeared stiffness technique and lamination parameters. 04 2010.

[31] P. Madabhusi-Raman and J. F. Davalos. Static shear correction factor for laminated rectangular beams. *Composites Part B: Engineering*, 27(3):285 – 293, 1996. doi: https://doi.org/10.1016/1359-8368(95)00014-3. Structural Composites in Infrastructures.

[32] C. McConnell and M. Duvelleroy. Airbus' majority stake in c series partnership with bombardier and investissement quebec comes into effect. `https://www.airbus.com/newsroom/press-releases/en/2018/07/airbus--majority-stake-in-c-series-partnership-with-bombardier-a.html`, 2018. [Online; accessed 7-July-2018].

[33] T. Megson. *Aircraft Structures for Engineering Students (Sixth Edition)*. Butterworth-Heinemann, sixth edition edition, 2017. doi: https://doi.org/10.1016/B978-0-08-100914-7.09992-8.

[34] C. Mittelstedt and W. Becker. *Strukturmechanik ebener Laminate /*. Studienbereich Mechanik, Technische Universität Darmstadt„ 1. auflage edition, Herbst 2016. ISBN 9783935868990.

[35] C. Mittelstedt and M. Beerhorst. Closed-form buckling analysis of compressively loaded composite plates braced by omega-stringers. *Composite Structures*, 88(3):424 – 435, 2009. doi: https://doi.org/10.1016/j.compstruct.2008.05.021.

[36] C. Mittelstedt and K.-U. Schröder. Local postbuckling of hat-stringer-stiffened composite laminated plates under transverse compression. *Composite Structures*, 92(12):2830 – 2844, 2010. doi: https://doi.org/10.1016/j.compstruct.2010.04.009.

[37] M. Nemeth. *A Treatise on Equivalent-plate Stiffnesses for Stiffened Laminated-composite Plates and Plate-like Lattices*. NASA technical paper. National Aeronautics and Space Administration, Langley Research Center, 2011.

[38] G. Norris. Dreamliner takes shape. `https://www.flightglobal.com/news/articles/dreamliner-takes-shape-207664/`, 2006. [Online; accessed 27-November-2017].

[39] G. Norris. 787-9 from the inside and 787 production update. `http://aviationweek.com/blog/787-9-inside-and-787-production-update`, 2013. [Online; accessed 7-July-2018].

[40] I. Orbital ATK. Commercial aircraft composite structures - fact sheet. `https://www.orbitalatk.com/flight-systems/aerospace-structures/`

commercial-aircraft-structures/docs/Commercial_Aircraft_Structures.pdf, 2017. [Online; accessed 27-November-2017].

[41] B. Rigby and T. Hepher. Factbox: Global supply chain for boeing's 787. https://www.reuters.com/article/us-hold-boeing-787-suppliers/factbox-global-supply-chain-for-boeings-787-idUSTRE4BA4LB20081211, 2008. [Online; accessed 7-July-2018].

[42] M. Ryan. Prime minister formally opens Bombardier's new wing facility in Belfast. http://uk.bombardier.com/en/media/newsList/details.bombardier-aerospace_20131011_primeministerformallyopensbombardi.bombardiercom.html, 2013. [Online; accessed 27-November-2017].

[43] A. S.A.S. Global market forcast. https://www.airbus.com/aircraft/market/global-market-forecast.html, 2017.

[44] D. Stamatelos, G. Labeas, and K. Tserpes. Analytical calculation of local buckling and post-buckling behavior of isotropic and orthotropic stiffened panels. *Thin-Walled Structures*, 49(3):422 – 430, 2011. doi: https://doi.org/10.1016/j.tws.2010.11.008.

[45] N. Stephen. Mindlin plate theory: Best shear coefficient and higher spectra validity. *Journal of Sound and Vibration*, 202(4):539 – 553, 1997. doi: https://doi.org/10.1006/jsvi.1996.0885.

[46] K. Svanberg. A class of globally convergent optimization methods based on conservative convex separable approximations. *SIAM Journal on Optimization*, pages 555–573.

[47] M. Tyrrell. C Series earns its wings. https://www.aero-mag.com/bombardier-c-series-cs100/, 2016. [Online; accessed 27-November-2017].

[48] M. Wagner and G. Norris. *Boeing 787 Dreamliner*. MBI Publishing Company, 2009. ISBN 9781616732271.

[49] E. Werthen and S. Dähne. Design rules consideration within optimization of composite structures using lamination parameters. 2016.

[50] J. Wiedemann. *Leichtbau: Elemente und Konstruktion*. Klassiker der Technik. Springer Berlin Heidelberg, 2006. ISBN 9783540336563.

[51] Z. Wu, G. Raju, and P. Weaver. Feasible region of lamination parameters for optimization of variable angle tow (vat) composite plates. 01 2013.

[52] Y. Xu, Y. Tong, M. Liu, and B. Suman. A new effective smeared stiffener method for global buckling analysis of grid stiffened composite panels. *Composite Structures*, 158:83 – 91, 2016. doi: https://doi.org/10.1016/j.compstruct.2016.09.015.

List of Figures

List of Tables

Appendix A

Transformation Matrices for CLT

As mentioned in Section 3.2.1, this appendix lists the required transformation matrices for the classical lamination theory, accordingly to Hahn and Tsai [22].

$$[\mathrm{T}_\sigma] \equiv \begin{bmatrix} \cos^2\varphi_S & \sin^2\varphi_S & 2\sin\varphi_S\cos\varphi_S \\ \sin^2\varphi_S & \cos^2\varphi_S & -2\sin\varphi_S\cos\varphi_S \\ -\sin\varphi_S\cos\varphi_S & \sin\varphi_S\cos\varphi_S & \cos^2\varphi_S - \sin^2\varphi_S \end{bmatrix} \tag{A.1a}$$

$$[\mathrm{T}_\sigma]^{-1} \equiv \begin{bmatrix} \cos^2\varphi_S & \sin^2\varphi_S & -2\sin\varphi_S\cos\varphi_S \\ \sin^2\varphi_S & \cos^2\varphi_S & 2\sin\varphi_S\cos\varphi_S \\ \sin\varphi_S\cos\varphi_S & -\sin\varphi_S\cos\varphi_S & \cos^2\varphi_S - \sin^2\varphi_S \end{bmatrix} \tag{A.1b}$$

$$[\mathrm{T}_\epsilon] \equiv \begin{bmatrix} \cos^2\varphi_S & \sin^2\varphi_S & \sin\varphi_S\cos\varphi_S \\ \sin^2\varphi_S & \cos^2\varphi_S & -\sin\varphi_S\cos\varphi_S \\ -2\sin\varphi_S\cos\varphi_S & 2\sin\varphi_S\cos\varphi_S & \cos^2\varphi_S - \sin^2\varphi_S \end{bmatrix} \tag{A.1c}$$

$$[\mathrm{T}_\epsilon]^{-1} \equiv \begin{bmatrix} \cos^2\varphi_S & \sin^2\varphi_S & -\sin\varphi_S\cos\varphi_S \\ \sin^2\varphi_S & \cos^2\varphi_S & \sin\varphi_S\cos\varphi_S \\ 2\sin\varphi_S\cos\varphi_S & -2\sin\varphi_S\cos\varphi_S & \cos^2\varphi_S - \sin^2\varphi_S \end{bmatrix} \tag{A.1d}$$

With the matrices in Equation (A.1) the global stiffness matrix of each play is defined with:

$$\overline{\mathbf{Q}} = \overline{\mathbf{T}}_\varepsilon^{-1}\mathbf{Q}\overline{\mathbf{T}}_\varepsilon \tag{A.2a}$$

$$\mathbf{Q} = \mathbf{T}_\varepsilon^{-1}\overline{\mathbf{Q}}\mathbf{T}_\varepsilon. \tag{A.2b}$$

Appendix B

Buckling Formulation for Restrained Boundary Conditions

The validation of the stiffened panel in Section 5 showed that the boundary conditions of the spacing span severely depends on the stiffening geometry. Therefore, Mittelstedt and Beerhorst [35] presented a closed-from analysis to determine the inter-stiffener critical buckling. It is implemented into the base code with:

$$N_{\mathrm{cr}} = \frac{8\pi^2}{w_{\mathrm{ss}}^2}\left(\sqrt{\frac{\tau_1}{\tau_2}}\sqrt{D_{11}D_{22}} + \frac{\tau_3}{\tau_2}\left(D_{12}+2D_{66}\right)\right), \qquad \text{(Eq. (46), reviewed)}$$

where

$$\tau_1 = 3D_{11}^2\pi^2 + 20kw_{\mathrm{ss}}D_{22} + 3k^2w_{\mathrm{ss}}^2 \tag{A.3a}$$

$$\tau_2 = 48D_{11}^2\pi^2 + 128kw_{\mathrm{ss}}D_{22} + 9k^2w_{\mathrm{ss}}^2, \tag{A.3b}$$

$$\tau_3 = 12D_{11}^2\pi^2 + 32kw_{\mathrm{ss}}D_{22} + 3k^2w_{\mathrm{ss}}^2 \tag{A.3c}$$

The stiffness terms D_{ij} correspond to either the skin's properties or the corrected stiffness matrix $\tilde{\boldsymbol{D}}$ from Equation (41) if a foot is present. The width w_{ss} represents the spacing span between the webs. The elastic restrained stiffness factor k is expressed as

$$k = \frac{3E_2I_2}{w_{\mathrm{ss}}\left(1+M_1-1/2M_2\right)}, \tag{A.4}$$

E_iI_I describe the local stiffness property of each element of the Ω stringer, i.e., left and right web, as well as the crown with:

$$E_iI_i = \frac{D_{11}D_{33}D_{33} - D_{11}D_{23}^2 - D_{12}^2D_{33} + 2D_{12}D_{13}D_{23} - D_{13}^2D_{22}}{D_{11}D_{33} - D_{13}^2}. \tag{A.5}$$

M_1 and M_2 are furthermore statically indeterminant moments with:

$$M_1 = \frac{\delta_{20}\delta_{12} - \delta_{10}\delta_{22}}{\delta_{11}\delta_{22} - \delta_{12}\delta_{21}} \tag{A.6a}$$

$$M_2 = \frac{\delta_{10}\delta_{21} - \delta_{20}\delta_{11}}{\delta_{11}\delta_{22} - \delta_{12}\delta_{21}}, \tag{A.6b}$$

where:

$$\delta_{10} = \frac{b_2}{3E_2I_2} \tag{A.7a}$$

$$\delta_{11} = \frac{b_1}{E_1I_1} + \frac{b_2}{3E_2I_2} \tag{A.7b}$$

$$\delta_{12} = -\frac{b_2}{6E_2I_2} \tag{A.7c}$$

$$\delta_{20} = -\frac{b_2}{6E_2I_2} \tag{A.7d}$$

$$\delta_{21} = -\frac{b_2}{6E_2I_2} \tag{A.7e}$$

$$\delta_{22} = \frac{b_2}{3E_2I_2} + \frac{b_3}{E_3I_3} \tag{A.7f}$$

With the previously mentioned equations, the critical buckling load is implemented into the base code and used for the evaluation of the critical buckling load of omega stiffened panels.

Appendix C

Equivalent-Plate Stiffness for T-Shaped Cross-Section

This appendix applies the derived equations from Chapter 3 to a skin panel, braced by T-shaped stringers. It is, analgously to the aforementioned chapter, separated into three parts. First the membrane stiffness is listed, then the bending stiffness and at the end the coupling between the previous two.

Equivalent Membrane Stiffness

$$(A_{11})_{\text{panel}} \equiv (A_{11})_{\text{skin}} + \frac{E_{\text{S}} A_{\text{S}}}{d_{\text{s}}} \tag{A.8a}$$

$$(A_{12})_{\text{panel}} \equiv (A_{12})_{\text{skin}} \tag{A.8b}$$

$$(A_{22})_{\text{panel}} \equiv (A_{22})_{\text{skin}} + \frac{w_{\text{foot}}}{d_{\text{s}}} (A_{22})_{\text{foot}} \tag{A.8c}$$

$$(A_{23})_{\text{panel}} \equiv (A_{23})_{\text{skin}} \tag{A.8d}$$

$$(A_{33})_{\text{panel}} \equiv \frac{d_{\text{s}}}{\dfrac{w_{\text{open skin}}}{(A_{33})_{\text{skin}}} + \dfrac{w_{\text{foot}}}{(A_{33})_{\text{skin + foot}}}} \tag{A.8e}$$

Equivalent Bending Stiffness

This section lists the equivalent bending stiffness for the present cross-section.

$$(D_{11})_{\text{panel}} \equiv (D_{11})_{\text{skin}} + \frac{E_{\text{S}} I^{\text{S}}_{\text{YY}}}{d_{\text{s}}} \tag{A.9a}$$

$$(D_{12})_{\text{panel}} \equiv (D_{12})_{\text{skin}} \tag{A.9b}$$

$$(D_{22})_{\text{panel}} \equiv (D_{22})_{\text{skin}} + \frac{w_{\text{foot}}}{d_{\text{s}}} \left((D_{22})_{\text{foot}} + d^2 \, (A_{22})_{\text{foot}} \right) \tag{A.9c}$$

$$(D_{23})_{\text{panel}} \equiv (D_{23})_{\text{skin}} \tag{A.9d}$$

$$(D_{33})_{\text{panel}} \equiv (D_{33})_{\text{skin}} + \frac{w_{\text{foot}}}{d_{\text{s}}} \left((D_{33})_{\text{foot}} + d^2 \, (A_{33})_{\text{foot}} \right) \tag{A.9e}$$

$$\tag{A.9f}$$

Equivalent Coupling Terms

This section lists the obtained coupling for the present cross-section.

$$(B_{11})_{\text{panel}} \equiv (B_{11})_{\text{skin}} + \frac{\overline{z} E_{\text{S}} A_{\text{S}}}{d_{\text{s}}} \tag{A.10a}$$

$$(B_{12})_{\text{panel}} \equiv (B_{12})_{\text{skin}} \tag{A.10b}$$

$$(B_{22})_{\text{panel}} \equiv (B_{22})_{\text{skin}} + \frac{w_{\text{foot}}}{d_{\text{s}}} \, (A_{22})_{\text{foot}} \tag{A.10c}$$

$$(B_{23})_{\text{panel}} \equiv (B_{23})_{\text{skin}} \tag{A.10d}$$

$$(B_{33})_{\text{panel}} \equiv (B_{33})_{\text{skin}} + \frac{w_{\text{foot}}}{d_{\text{s}}} \, (A_{33})_{\text{foot}} \tag{A.10e}$$

Appendix D

Equivalent-Plate Stiffness for I-Shaped Cross-Section

This appendix applies the derived equations from Chapter 3 to a skin panel, braced by I-shaped stringers. It is, analgously to the aforementioned chapter, separated into three parts. First the membrane stiffness is listed, then the bending stiffness and at the end the coupling between the previous two.

Equivalent Membrane Stiffness

This section lists the equivalent membrane stiffness for the present cross-section.

$$(A_{11})_{\text{panel}} \equiv (A_{11})_{\text{skin}} + \frac{E_{\text{S}} A_{\text{S}}}{d_{\text{s}}} \tag{A.11a}$$

$$(A_{12})_{\text{panel}} \equiv (A_{12})_{\text{skin}} \tag{A.11b}$$

$$(A_{22})_{\text{panel}} \equiv (A_{22})_{\text{skin}} + \frac{w_{\text{foot}}}{d_{\text{s}}} (A_{22})_{\text{foot}} \tag{A.11c}$$

$$(A_{23})_{\text{panel}} \equiv (A_{23})_{\text{skin}} \tag{A.11d}$$

$$(A_{33})_{\text{panel}} \equiv \frac{d_{\text{s}}}{\dfrac{w_{\text{open skin}}}{(A_{33})_{\text{skin}}} + \dfrac{w_{\text{foot}}}{(A_{33})_{\text{skin + foot}}}} \tag{A.11e}$$

Equivalent Bending Stiffness

This section lists the equivalent bending stiffness for the present cross-section.

$$(D_{11})_{\text{panel}} \equiv (D_{11})_{\text{skin}} + \frac{E_{\text{S}} I^{\text{S}}_{\text{YY}}}{d_{\text{s}}} \tag{A.12a}$$

$$(D_{12})_{\text{panel}} \equiv (D_{12})_{\text{skin}} \tag{A.12b}$$

$$(D_{22})_{\text{panel}} \equiv (D_{22})_{\text{skin}} + \frac{w_{\text{foot}}}{d_{\text{s}}} \left((D_{22})_{\text{foot}} + d^2 \, (A_{22})_{\text{foot}} \right) \tag{A.12c}$$

$$(D_{23})_{\text{panel}} \equiv (D_{23})_{\text{skin}} \tag{A.12d}$$

$$(D_{33})_{\text{panel}} \equiv (D_{33})_{\text{skin}} + \frac{w_{\text{foot}}}{d_{\text{s}}} \left((D_{33})_{\text{foot}} + d^2 \, (A_{33})_{\text{foot}} \right) \tag{A.12e}$$

$$\tag{A.12f}$$

Equivalent Coupling Terms

This section lists the obtained coupling for the present cross-section.

$$(B_{11})_{\text{panel}} \equiv (B_{11})_{\text{skin}} + \frac{\overline{z} E_{\text{S}} A_{\text{S}}}{d_{\text{s}}} \tag{A.13a}$$

$$(B_{12})_{\text{panel}} \equiv (B_{12})_{\text{skin}} \tag{A.13b}$$

$$(B_{22})_{\text{panel}} \equiv (B_{11})_{\text{skin}} + \frac{w_{\text{foot}}}{d_{\text{s}}} \left((A_{22})_{\text{foot}} \right) \tag{A.13c}$$

$$(B_{23})_{\text{panel}} \equiv (B_{23})_{\text{skin}} \tag{A.13d}$$

$$(B_{33})_{\text{panel}} \equiv (B_{33})_{\text{skin}} + \frac{w_{\text{foot}}}{d_{\text{s}}} \left((A_{33})_{\text{foot}} \right) \tag{A.13e}$$

Appendix E

Equivalent-Plate Stiffness for Omega-Shaped Cross-Section

This appendix applies the derived equations from Chapter 3 to a skin panel, braced by Ω-shaped stringers. It is, analgously to the aforementioned chapter, separated into three parts. First the membrane stiffness is listed, then the bending stiffness and at the end the coupling between the previous two.

Equivalent Membrane Stiffness

This section lists the equivalent membrane stiffness for the present cross-section.

$$(A_{11})_{\text{panel}} \equiv (A_{11})_{\text{skin}} + \frac{E_{\text{S}} A_{\text{S}}}{d_{\text{s}}} \tag{A.14a}$$

$$(A_{12})_{\text{panel}} \equiv (A_{12})_{\text{skin}} \tag{A.14b}$$

$$(A_{22})_{\text{panel}} \equiv (A_{22})_{\text{skin}} + \frac{w_{\text{foot}}}{d_{\text{s}}} (A_{22})_{\text{foot}} \tag{A.14c}$$

$$(A_{23})_{\text{panel}} \equiv (A_{23})_{\text{skin}} \tag{A.14d}$$

$$(A_{33})_{\text{panel}} \equiv \frac{d_{\text{s}}}{\dfrac{w_{\text{open skin}}}{(A_{33})_{\text{skin}}} + \dfrac{2w_{\text{foot}}}{(A_{33})_{\text{skin + foot}}} + \dfrac{w_{\text{crown}}}{(A_{33})_{\text{crown}}}} \tag{A.14e}$$

Equivalent Bending Stiffness

This section lists the equivalent bending stiffness for the present cross-section.

$$(D_{11})_{\text{panel}} \equiv (D_{11})_{\text{skin}} + \frac{E_{\text{S}} I_{\text{YY}}^{\text{S}}}{d_{\text{s}}} \tag{A.15a}$$

$$(D_{12})_{\text{panel}} \equiv (D_{22})_{\text{skin}} \tag{A.15b}$$

$$(D_{22})_{\text{panel}} \equiv (D_{22})_{\text{skin}} + \frac{2w_{\text{foot}}}{d_{\text{s}}} \left((D_{22})_{\text{foot}} + d^2 \, (A_{22})_{\text{foot}} \right) \tag{A.15c}$$

$$+ \left(\frac{2(D_{22})_{\text{skin}} w_{\text{cs}}}{(D_{22}) w_{\text{web}}} + \frac{2(D_{22})_{\text{crown}} w_{\text{cs}}}{(D_{22})_{\text{skin}} w_{\text{foot}}} \right) \cdot \frac{2(D_{22})_{\text{skin}} w_{\text{cs}}}{d_s} \tag{A.15d}$$

$$(D_{23})_{\text{panel}} \equiv (D_{23})_{\text{skin}} \tag{A.15e}$$

$$(D_{33})_{\text{panel}} \equiv (D_{33})_{\text{skin}} + \frac{w_{\text{foot}}}{d_{\text{s}}} \left((D_{33})_{\text{foot}} + d^2 \, (A_{33})_{\text{foot}} \right) \tag{A.15f}$$

$$+ \frac{\dfrac{A^2}{d_s}}{G_{\text{f}} + \sum\limits_{j=1}^{n} \dfrac{w_j}{A_{33,j}}} \tag{A.15g}$$

Equivalent Coupling Terms

This section lists the obtained coupling for the present cross-section.

$$(B_{11})_{\text{panel}} \equiv (B_{11})_{\text{skin}} + \frac{\overline{z} E_{\text{S}} A_{\text{S}}}{d_{\text{s}}} \tag{A.16a}$$

$$(B_{12})_{\text{panel}} \equiv (B_{12})_{\text{skin}} \tag{A.16b}$$

$$(B_{22})_{\text{panel}} \equiv (B_{22})_{\text{skin}} + \frac{w_{\text{foot}}}{d_{\text{s}}} \, (A_{22})_{\text{foot}} \tag{A.16c}$$

$$(B_{23})_{\text{panel}} \equiv (B_{23})_{\text{skin}} \tag{A.16d}$$

$$(B_{33})_{\text{panel}} \equiv (B_{33})_{\text{skin}} + \frac{w_{\text{foot}}}{d_{\text{s}}} \, (A_{33})_{\text{foot}}) \tag{A.16e}$$

$$+ A_{\text{cell}} q_{\text{cr}} \frac{(A_{33})_{\text{panel}}}{d_{\text{s}}} \tag{A.16f}$$